AD-A181 122 OUTSTANDING PROBLEMS IN HIGH POWER PULSED LASER/TARGET INTERACTIONS(U) S-CUBED LA JOLLA CA B E FREEMAN ET AL. 26 AUG 86 SSS-RR-8123 DNA-TR-86-299 DNA001-83-C-0201 1/1

UNCLASSIFIED F/G 9/3 NL

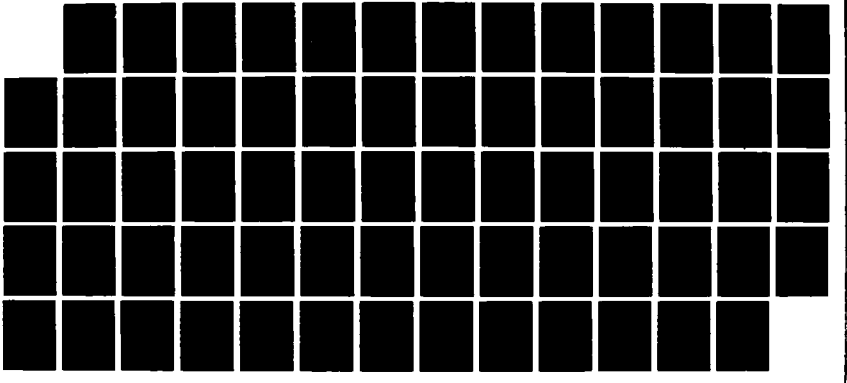

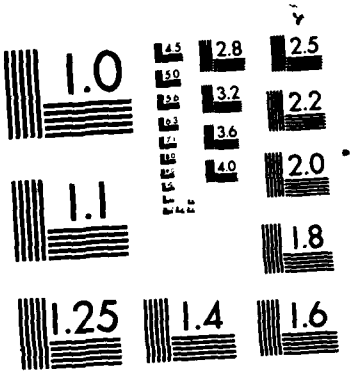

MICROCOPY RESOLUTION TEST CHART
NATIONAL BUREAU OF STANDARDS-1963-A

DNA-TR-86-299

OUTSTANDING PROBLEMS IN HIGH POWER PULSED LASER/TARGET INTERACTIONS

B. E. Freeman
P. C. Patnaik
S-CUBED
A Division of Maxwell Laboratories, Inc.
P. O. Box 1620
La Jolla, CA 92038-1620

26 August 1986

Technical Report

CONTRACT No. DNA 001-83-C-0281

Approved for public release;
distribution is unlimited.

THIS WORK WAS SPONSORED BY THE DEFENSE NUCLEAR AGENCY
UNDER RDT&E RMSS CODE B342083466 N99QAXAK00050 H2590D.

Prepared for
Director
DEFENSE NUCLEAR AGENCY
Washington, DC 20305-1000

Destroy this report when it is no longer needed. Do not return to sender.

PLEASE NOTIFY THE DEFENSE NUCLEAR AGENCY ATTN: TITL, WASHINGTON, DC 20305 1000, IF YOUR ADDRESS IS INCORRECT, IF YOU WISH IT DELETED FROM THE DISTRIBUTION LIST, OR IF THE ADDRESSEE IS NO LONGER EMPLOYED BY YOUR ORGANIZATION.

DISTRIBUTION LIST UPDATE

This mailer is provided to enable DNA to maintain current distribution lists for reports. We would appreciate your providing the requested information.

- ☐ Add the individual listed to your distribution list.
- ☐ Delete the cited organization/individual.
- ☐ Change of address.

NAME: _____

ORGANIZATION: _____

OLD ADDRESS	CURRENT ADDRESS
_____	_____
_____	_____
_____	_____

TELEPHONE NUMBER: ( ) _____

SUBJECT AREA(s) OF INTEREST:

_____	_____
_____	_____
_____	_____

DNA OR OTHER GOVERNMENT CONTRACT NUMBER: _____

CERTIFICATION OF NEED-TO-KNOW BY GOVERNMENT SPONSOR (if other than DNA):

SPONSORING ORGANIZATION: _____

CONTRACTING OFFICER OR REPRESENTATIVE: _____

SIGNATURE: _____

CUT HERE AND RETURN

Director
Defense Nuclear Agency
ATTN: [redacted] TITL
Washington, DC 20305-1000

Director
Defense Nuclear Agency
ATTN: [redacted] TITL
Washington, DC 20305-1000

UNCLASSIFIED
SECURITY CLASSIFICATION OF THIS PAGE

ADA181122

REPORT DOCUMENTATION PAGE

1a. REPORT SECURITY CLASSIFICATION UNCLASSIFIED	1b RESTRICTIVE MARKINGS
2a. SECURITY CLASSIFICATION AUTHORITY N/A since Unclassified	3 DISTRIBUTION / AVAILABILITY OF REPORT Approved for public release; distribution is unlimited.
2b. DECLASSIFICATION / DOWNGRADING SCHEDULE N/A since Unclassified	
4 PERFORMING ORGANIZATION REPORT NUMBER(S) SSS-RR-8123	5 MONITORING ORGANIZATION REPORT NUMBER(S) DNA-TR-86-299
6a NAME OF PERFORMING ORGANIZATION S-CUBED, A Division of Maxwell Laboratories, Inc.	6b OFFICE SYMBOL (If applicable)
6c. ADDRESS (City, State, and ZIP Code) P.O. Box 1620 La Jolla, CA 92038-1620	7a NAME OF MONITORING ORGANIZATION Director Defense Nuclear Agency
	7b ADDRESS (City, State, and ZIP Code) Washington, DC 20305-1000
8a. NAME OF FUNDING / SPONSORING ORGANIZATION	8b. OFFICE SYMBOL (If applicable) SPAS/Wolf
	9 PROCUREMENT INSTRUMENT IDENTIFICATION NUMBER DNA 001-83-C-0281
8c. ADDRESS (City, State, and ZIP Code)	10 SOURCE OF FUNDING NUMBERS

PROGRAM ELEMENT NO	PROJECT NO	TASK NO	WORK UNIT ACCESSION NO
62715H	N99QAXA	K	DH007164

11 TITLE (Include Security Classification)
OUTSTANDING PROBLEMS IN HIGH POWER PULSED LASER/TARGET INTERACTIONS

12 PERSONAL AUTHOR(S)
Freeman, B. E. and Patnaik, P. C.

13a TYPE OF REPORT	13b TIME COVERED	14 DATE OF REPORT (Year, Month, Day)	15 PAGE COUNT
Technical	FROM 830928 TO 840731	860826	64

16 SUPPLEMENTARY NOTATION
This work was sponsored by the Defense Nuclear Agency under RDT&E RMSS Code B342083466 N99QAXAK00050 H2590D.

17 COSATI CODES		
FIELD	GROUP	SUB-GROUP
9	3	
19	5	

18 SUBJECT TERMS (Continue on reverse if necessary and identify by block number)
Laser Beam in Air
Laser-Supported Radiation Wave
Laser-Target Interaction

19 ABSTRACT (Continue on reverse if necessary and identify by block number)

An investigation was made of the interaction of a high-power laser beam with a target in air. A laser-supported radiation wave in the air is predicted. Models of this process were developed. An analytic model of the steady-state was compared with a transient numerical model using a one-dimensional radiation/hydrodynamic code. Comparisons with data indicate agreement for Nd-glass frequency laser radiation, but discrepancies for CO_2 laser frequency. Speculations are made about the source of the discrepancy.

20 DISTRIBUTION / AVAILABILITY OF ABSTRACT	21 ABSTRACT SECURITY CLASSIFICATION
☐ UNCLASSIFIED/UNLIMITED ☒ SAME AS RPT ☐ DTIC USERS	UNCLASSIFIED
22a NAME OF RESPONSIBLE INDIVIDUAL Sandra E. Young	22b TELEPHONE (Include Area Code) (202) 325-7042
	22c OFFICE SYMBOL DNA/CSTI

DD FORM 1473, 84 MAR 83 APR edition may be used until exhausted
All other editions are obsolete

SECURITY CLASSIFICATION OF THIS PAGE
UNCLASSIFIED

Conversion Table

Conversion factors for U.S. Customary to metric (SI) units of measurement

MULTIPLY → / ← TO GET	BY → / ← BY	TO GET → / ← DIVIDE
angstrom	1.000 000 X E -10	meters (m)
atmosphere (normal)	1 013 25 X E +2	kilo pascal (kPa)
bar	1.000 000 X E +2	kilo pascal (kPa)
barn	1 000 000 X E -28	meter^2 (m^2)
British thermal unit (thermochemical)	1.054 350 X E +3	joule (J)
calorie (thermochemical)	4 184 000	joule (J)
cal (thermochemical)/cm^2	4 184 000 X E -2	mega joule/m^2 (MJ/m^2)
curie	3 700 000 X E +1	*giga becquerel (GBq)
degree (angle)	1 745 329 X E -2	radian (rad)
degree Fahrenheit	t_K = (t°F + 459 67)/1. 8	degree kelvin (K)
electron volt	1. 602 19 X E -19	joule (J)
erg	1.000 000 X E -7	joule (J)
erg/second	1.000 000 X E -7	watt (W)
foot	3. 048 000 X E -1	meter (m)
foot-pound-force	1. 355 818	joule (J)
gallon (U S liquid)	3 785 412 X E -3	meter^3 (m^3)
inch	2 540 000 X E -2	meter (m)
jerk	1 000 000 X E +9	joule (J)
joule/kilogram (J/kg) (radiation dose absorbed)	1.000 000	Gray (Gy)
kilotons	4. 183	terajoules
kip (1000 lbf)	4. 448 222 X E +3	newton (N)
kip/inch^2 (ksi)	6 894 757 X E +3	kilo pascal (kPa)
ktap	1 000 000 X E +2	newton-second/m^2 ($N-s/m^2$)
micron	1 000 000 X E -6	meter (m)
mil	2. 540 000 X E -5	meter (m)
mile (international)	1. 609 344 X E +3	meter (m)
ounce	2. 834 952 X E -2	kilogram (kg)
pound-force (lbs avoirdupois)	4. 448 222	newton (N)
pound-force inch	1 129 848 X E -1	newton-meter (N·m)
pound-force/inch	1 751 268 X E +2	newton/meter (N/m)
pound-force/foot^2	4 788 026 X E -2	kilo pascal (kPa)
pound-force/inch^2 (psi)	6 894 757	kilo pascal (kPa)
pound-mass (lbm avoirdupois)	4. 535 924 X E -1	kilogram (kg)
pound-mass-foot^2 (moment of inertia)	4 214 011 X E -2	kilogram-meter^2 ($kg \cdot m^2$)
pound-mass/foot^3	1 601 846 X E +1	kilogram/meter^3 (kg/m^3)
rad (radiation dose absorbed)	1 000 000 X E -2	**Gray (Gy)
roentgen	2 579 760 X E -4	coulomb/kilogram (C/kg)
shake	1 000 000 X E -8	second (s)
slug	1. 459 390 X E +1	kilogram (kg)
torr (mm Hg, 0° C)	1. 333 22 X E -1	kilo pascal (kPa)

*The becquerel (Bq) is the SI unit of radioactivity, 1 Bq = 1 event/s
**The Gray (Gy) is the SI unit of absorbed radiation.

TABLE OF CONTENTS

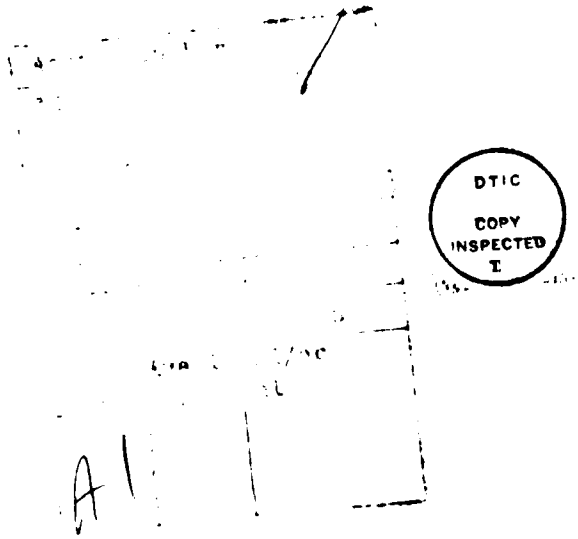

LIST OF ILLUSTRATIONS

SECTION 1
INTRODUCTION

The Defense Nuclear Agency (DNA) High Energy Pulsed Laser program contained coordinated high power laser beam/target interaction experiments and model-based interpretations. The experimental data base includes a number of parameters such as target material, air density, laser power, pulse length, frequency, and spot size.

Within this effort interaction modeling work can play several important roles:

1. Models can distill the experimental data base and provide an interpolation tool for cases spanned by the data.

2. Models can elucidate the physical processes taking place in the interaction and quantify their importance to target impulse and heating.

3. Models can provide suggestions to the experimental program on how to critically test the models and how optimum experimental parameters may be selected.

4. Ultimately, models can yield a quantitative data base for interpolation and extrapolation in the design of a system. It can also guide the design of systems tests.

Our major interest in this program is in the regime in which an air plasma is formed. In this environment there are a number of processes to be taken into account.

1. Starting from plasma initiation, the laser beam is partially or totally absorbed by the plasma and heats it.

2. The target is correspondingly shielded from the laser beam. The hot plasma is supported hydrodynamically by the target and sends signals into the surrounding air. One dimensional hydrodynamic effects include the laser combustion (LSC) and detonation (LSD) waves. Multi-dimensional hydrodynamic effects arise from lateral expansion of the heated region over a small spot size and from nonnormal beam incidence.

3. Conduction and electron diffusion redistribute energy within the plasma and heat the target.

4. Radiative transfer redistributes energy within the plasma, may propagate a super-detonation wave, cools the plasma by emission and heats the target. If the target is heated to a high enough temperature it also may reradiate, ablate and further generate impulse, or both.

The role of each of the above processes depends on the values of the parameters specifying the interaction. One energy transport mechanism will tend to predominate over all others within a range of parameter values. Initially the models employed heuristic descriptions of plasma initiation, postulated that a sharp-fronted laser supported detonation (LSD) is established, and accounted for lateral expansion effects via analytic expressions. Beam absorption over an extended distance, energy conduction and reradiation processes and target albedo and vaporization effects were not included. The objective of this investigation is to research several of these problems from a theoretical approach. In the following paragraphs we discuss them more quantitatively.

There are three different radiative effects which are useful to distinguish:

1. Radiation can cool the plasma by removing energy from the plasma region.

2. Radiation can transport energy to the target itself, increasing target heating and possibly resulting in target vaporization and blow-off.

3. A radiation-dominated super-detonated wave can displace the zone of plasma heating away from the target to increase radiative and hydrodynamic geometrical losses.

Unheated air outside of the plasma zone is substantially transparent to photons having energies in a window below ~7 eV.

Consequently, a fraction of photons radiated by the plasma in directions away from the target will be lost from the interaction. In the range of intensities of interest (10^7 - 10^{10} w/cm^2) plasma temperatures are sufficiently high in the LSC and LSD waves such that radiation can remove a significant fraction of the plasma energy in the time of the interaction. We have estimated that the plasmas are also sufficiently thin so that a part of this energy can escape the source region. Small spot sizes enhance the escape probability.

Reradiation from the plasma into half of the solid angle may impinge on the target both inside of the spot area and in the peripheral area. Substantially increased heating of high reflectance targets takes place due to this source since a higher fraction of these energetic photons is absorbed. While reradiation is credited with an enhanced thermal coupling coefficient in the LSC regime,[1] it is also possible that the increased heating may produce vaporization. Due to cooling by thermal conduction in the target it requires an excessive time to initiate vaporization of aluminum at 10^7 w/cm^2, but the time becomes comparable to or smaller than typical pulse durations for beam intensities of 10^8 w/cm^2 and greater. Target vapor blow-off contributions to the impulse were inferred[2] for aluminum and nonmetallic targets near the threshold for LSD initiation. While the vaporization rate will fall off due to vapor shielding in the LSD regime, a significant blow-off impulse should also be present under these conditions from reradiation.

When the LSD wave plasma becomes hotter as laser power density is increased, reradiation from the wave can preheat the zone within the beam just ahead of the shock. When the ionization within this region becomes sufficient to initiate absorption of the beam a super-detonation wave is initiated. This faster moving absorption front depends on plasma reradiation to transport energy and sustain the wave. It is likely that the super-detonation wave will decrease the

impulse at the target, since the beam energy will be deposited farther from the target surface where lateral expansion and radiation will dissipate the pressure. This process was first identified and qualitatively modeled by Raizer.[3] He found that for air, the front speed is not much greater than for the LSD, and that its dependence on power density is only slightly stronger. This seems to imply that the threshold for the super-detonation wave is very high. Observations, whoever, suggest that the super-detonation takes place at lower power densities. Pirri, *et al.*[4] interpret streak photographs from one of the NRL experiments at ~10^8 w/cm^2 to indicate a frontal speed approximately two times greater than LSD and suggest that radiation may be responsible. Markovich, *et al.*[5] find a speed three times higher than for an LSD if the power density is greater than 10^9 w/cm^2. In other gases there are observations of higher propagation speeds as well. In argon and xenon[6] using a CO_2 laser the threshold for super-detonation was found to be 3-4 x 10^7 w/cm^2 and the speed increased faster than the square of the laser power. In xenon[7] using a neodymium glass laser, super-detonation took place at 4 x 10^7 w/cm^2.

There appears to be considerable uncertainty about the super-detonation regime from the point-of-view of theory. Only a few estimates have been made, and these do not adequately take into account the rapidly changing frequency dependence of absorption coefficients as the temperature of the gas changes. Numerical calculations[8] in plane geometry of superdetonation waves in one-tenth ambient density air at Nd-glass frequency and power densities q_o = 0.4 - 2.5 x 10^9 w/cm^2 have been reviewed. In the indicated range of laser power density these authors find that a radiative precursor moves away from the target at speeds higher than the LSD speed. At 0.4 x 10^9 w/cm^2, however, the precursor is formed slowly from the LSD wave, indicating that the threshold for superdetonation is being approached. They also develop a simple theory which, in agreement

with their calculations, gives a superdetonation speed $D \sim q_o^{0.71}$. This is a stronger dependence on power density than for the LSD which gives $D_c \sim q_o^{1/3}$.

The lowering of the threshold for the ignition of an air plasma by a laser due to the proximity of the target surface has been the subject of extensive observations and theoretical study. The results of this work have been characterized as requiring that a threshold fluence and a threshold flux be incident on the target. There is as yet an incomplete understanding of these important rules. Any delay in plasma ignition, for typical pulse durations, is likely to translate into significantly less energy being coupled to the target with commensurate lowering of I/E ratios.

A model [9] which has been developed to correlate these data on metallic targets invokes laser-induced breakdown of target vapor, following the vaporization of surface-indulated flakes of the target by laser heating. While the treatment of target vapor breakdown is quite plausible, the model of the initial ionization via vaporization is only one of several postulated initiation mechanisms. In addition, the postulated density, thickness and area of the flakes affects the quantitative behavior of the model.

In view of the significant role of plasma ignition in the coupling of laser power to target impulse it is important that models of ignition be as reliable as possible. In particular, it is desirable to reduce the dependence of the result on *ad hoc* parameters of the model.

In many problems of interest several factors which are not simulated in the current experimental program will be present. A turbulent boundary layer containing shocked and sheared air may exist over the target and the beam in general will not be normally incident on it. The target material may also be appreciably heated.

Several of the effects of the boundary layer can be accounted for rather simply. For example, oblique incidence of the beam having a large spot size can be equated to a normally incident beam of a lower power and lower laser frequency. Boundary layer compression and heating effects on the plasma wave propagation are also modeled in a straightforward manner.

The role of the aerodynamic boundary layer on plasma initiation and the effects of shear flow and turbulence on wave propagation appear not to have been investigated for high energy pulsed lasers.

Obliquely incident small spot size beams will be accompanied by a more complicated hydrodynamic flow and radiative interaction. This interaction will tend to displace the center of the target interaction toward the up-beam direction.

In the following sections we report on the work carried out during the investigation. The major tasks have been the modeling of the LSR wave in air. Central to the study is the determination of air optical properties; these are described in Section 2. The LSR wave has been modeled by two complementary techniques. The development of an analytic study wave model and the evaluation of a numerical model, together with comparisons with experimental data, are described in Section 3.

SECTION 2
OPTICAL PROPERTIES OF AIR

2.1 SELF-RADIATION FROM THE AIR PLASMA.

The interaction of the hot air plasma with the target and the possible propagation of the LSR mode depend on the transport of radiation originating in the emission of hot air and its subsequent transport through the air. For the times and distances of interest in high-power pulsed lasers, it is not possible to substantially simplify this transport description by making the diffusion approximation (involving the Rosseland mean free path) or the emission approximation (requiring the Planck mean free path). For the plasmas of interest the air may be optical thick in certain frequency ranges, optically thin or of intermediate thickness in other frequencies. This circumstance requires that air absorption coefficients as a function of frequency for a range of temperature and density of interest be obtained. The data must span the temperature range of ambient to ~ 10 eV and have the corresponding frequency resolution. The data were located and obtained from the Los Alamos National Laboratory. A computer tape which contains group absorption coefficients, as well as Planck and Rosseland mean opacities, for a grid of temperatures and densities covering the range of interest has been received and processed. Two frequency groupings are available: a 19-group and a 30-group data set. These data provide the required input information. In principle, the above data should also suffice for the absorption of laser radiation by heated air. However, in fact they are inadequate because a) the laser frequencies of interest are not resolved in the data, and b) the free-free absorption by atoms and molecules is not included (only ionic free-free has been considered). We have decided to evaluate these absorption coefficients in a special subroutine.

2.2 LASER BEAM ABSORPTION.

Absorption coefficients of air for temperatures of a few electron volts and ambient and lower densities are required in order to simulate existing laser experiments.

For the laser beam our initial application is to a Nd-glass laser having photon energy $h\nu = 1.16$ eV, where the absorption coefficient results from free-free and high-lying bound-free transitions. We have evaluated the absorption coefficient for cases of interest in the absorption of the laser beam. The problem consists of two parts: the evaluation of (equilibrium) concentrations of species, and the calculation of the corresponding absorption coefficients. We have employed results of calculations of the composition of low temperature equilibrium air kindly provided to us by F. Gilmore (private communication). These data include molecular, atomic and ionic species and employ a detailed description of excited states in the partition functions. Using these data as input, a computer code was written to evaluate the contributions of:

1. Free-free transitions in ions.
2. The correction to account for absorption in high-lying bound states.
3. Free-free transitions in the field of the predominant neutral species (which are important below ~ 1.5 eV).

This calculation employs the formulation by Dalgarno and Lane[10] for neutral free-free absorption and the corrections to the ionic free-free absorption of N^+ and O^+ by Peach.[11] Data for nonhydrogenic corrections to more highly ionized species are not available; we expect the corrections to be smaller for them and, in any event, to make a smaller contribution to the absorption coefficient in the toe transition region. Molecular band absorption, which may contribute to

the absorption coefficient at temperatures less than 1 eV, is currently neglected.

The total absorption coefficient μ_ℓ evaluated at $h\nu = 1.16$ eV is shown as a function of temperature θ in Figure 1 for standard air density and in Figure 2 for 0.1 times standard density. This quantity is a strongly increasing function of temperature, a property which decreases the sensitivity of the final result to its accuracy. It will be seen below that the most important temperature range for the LSR wave at standard air density is 1.5 - 2.0 eV. It is also possible to calculate μ_ℓ for other choices of laser frequency and density.

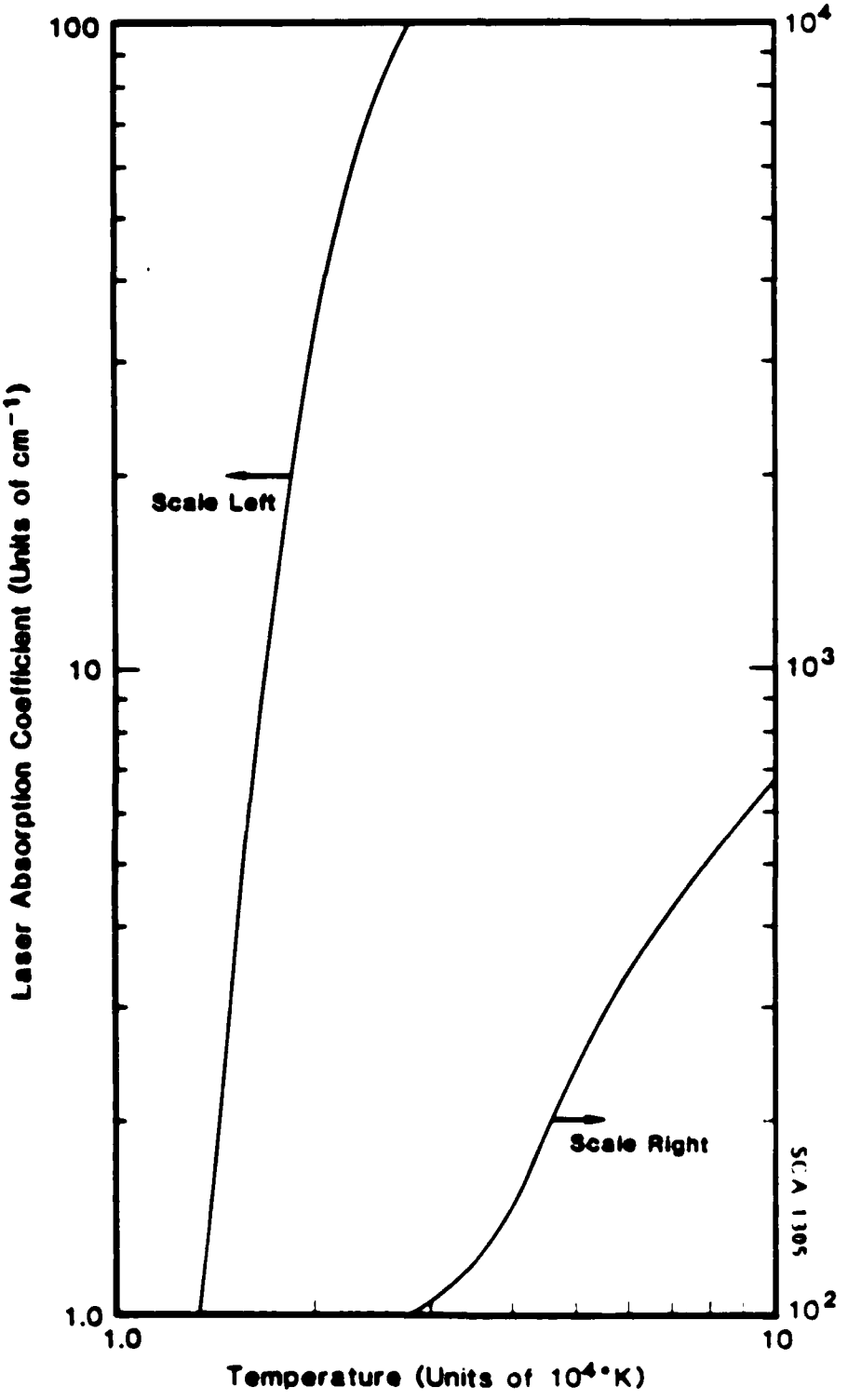

Figure 1. Laser absorption coefficient of air versus temperature for density 1.29×10^{-3} gm/cm^3 and laser frequency = 1.16 eV.

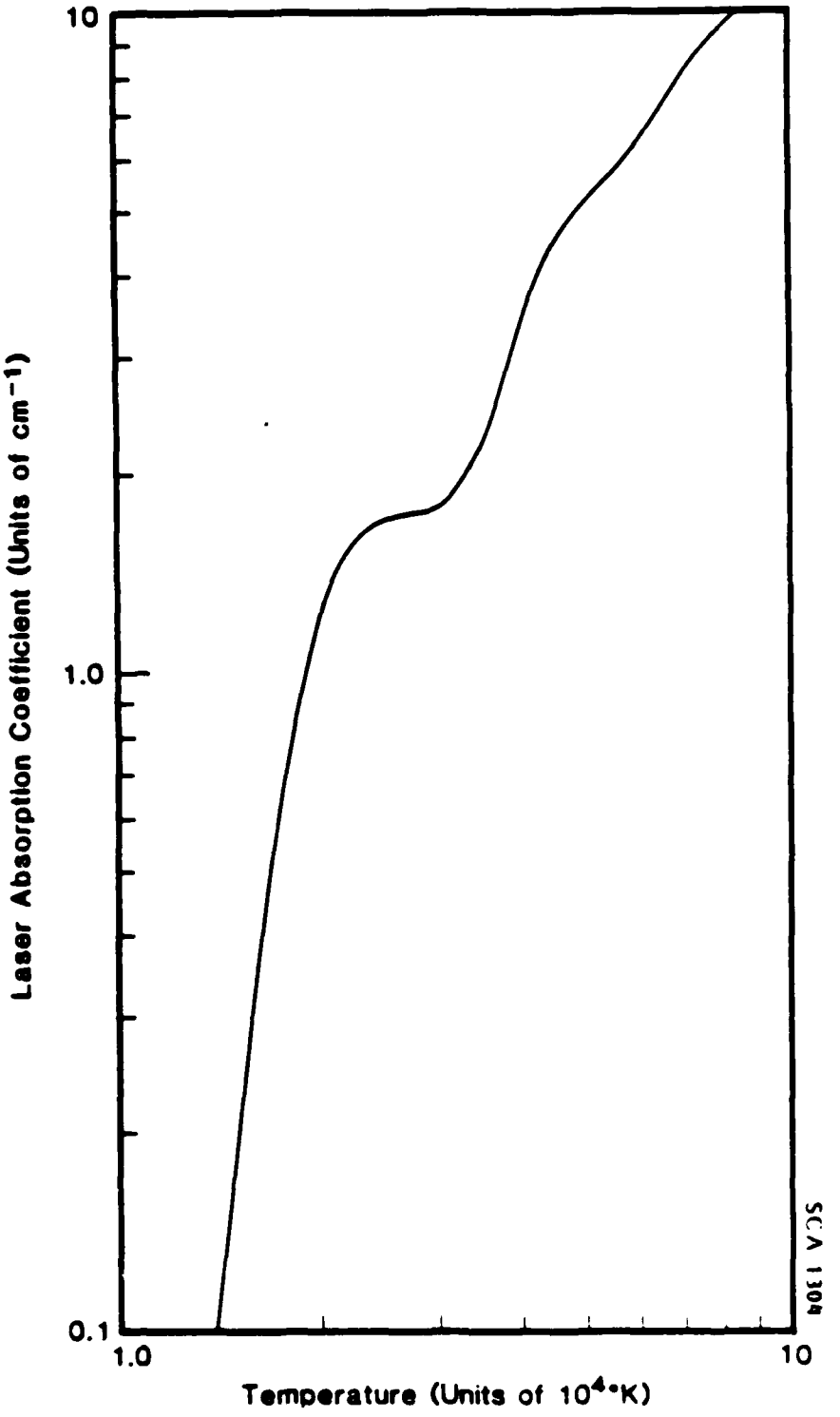

Figure 2. Laser absorption coefficient of air versus temperature for density 1.29×10^{-4} gm/cm^3 and laser frequency = 1.16 eV.

SECTION 3
LSR WAVES IN AIR

The radiation-supported radiation (LSR) wave mode of target interaction depends on radiation transport to replace the shock wave of the LSD mode as the energy transporting mechanism. With sufficiently high laser power a threshhold is reached in which the heated plasma emits radiation at a rate and with a frequency such that the laser beam is absorbed ahead of the shock wave. In this section we investigate this process for a noninteractive target in an air atmosphere.

Two different approaches were employed in the study: a qualitative steady-state model was developed, and a radiation/hydrodynamic numerical model was adapted to perform quantitative calculations of the transient interaction. The two approaches are complementary to each other in developing an understanding of the LSR phenomenon.

3.1 A STEADY-STATE ANALYTIC MODEL.

A simplified model of the steady propagation of a laser-supported radiation wave in air was developed. The model is based on the formation of a self-radiation-heated precursor ahead of the laser-heated main wave. Applied to air at sea-level density and Nd-glass frequency, the laser supported radiation (LSR) model propagates faster than the laser supported detonation (LSD) wave for speeds greater than 2.4×10^6 cm/s.

The formulation of the analytic model, results from evaluating it and comparisons with data are recorded in a topical report.[12] This report, SSS-R-84-6416, entitled "Laser Supported Radiation Waves in Air-Analytic Correlations," is appended to this document. For a

detailed account of the model the reader should refer to this report. Briefly, the comparison of model calculations with the data are outlined below.

Evaluating the model for $h\nu = 1.17$ eV (Nd-glass laser frequency) and for $(\rho_o/\rho_\infty) = 0.1,\ 1.0$ the wave speed dependence on laser flux is shown in Figure 3 (long-dashed curves). For comparison are the corresponding relations for a steady LSD wave (full curves). Also shown (open circles) are data from the experiments of Reference 13, using a Nd-glass laser. The trend of the high-fluence data is reproduced by the model not only in slope but also in magnitude (i.e., there are no adjustable constants within the model; however, the data have been plotted, somewhat arbitrarily, against peak power density). The slope of the theoretical curve for standard density is almost identical with that proposed in Reference 8 on the basis of numerical calculations and a partial theory applied to air of one-tenth normal density. Our calculation for this density displays a steeper slope and is not in good agreement with the calculations of Reference 8 (open squares). Furthermore, in contrast to the normal density case, examination of intermediate results indicates that, especially at the lower flux levels, the assumptions within the model are not well satisfied (the precursor temperature becomes comparable with the main wave temperature). Consequently, the model cannot be confidently applied for Nd-glass at densities of 0.1 normal or less. The apparent agreement between numerical calculations, and this type of model in Reference 8 should be regarded with reservations.

The model can be applied at other laser frequencies as well. We carried out a calculation at CO_2 laser frequency (10.6 μm) for standard density air; the result is shown in Figure 3 as the short-dashed curve. The model indicates that the wave speed curve is shifted with approximately the same slope to somewhat lower power densities. Under these conditions the range of validity of the theory will also extend to somewhat lower densities, because the precursor temperatures are smaller.

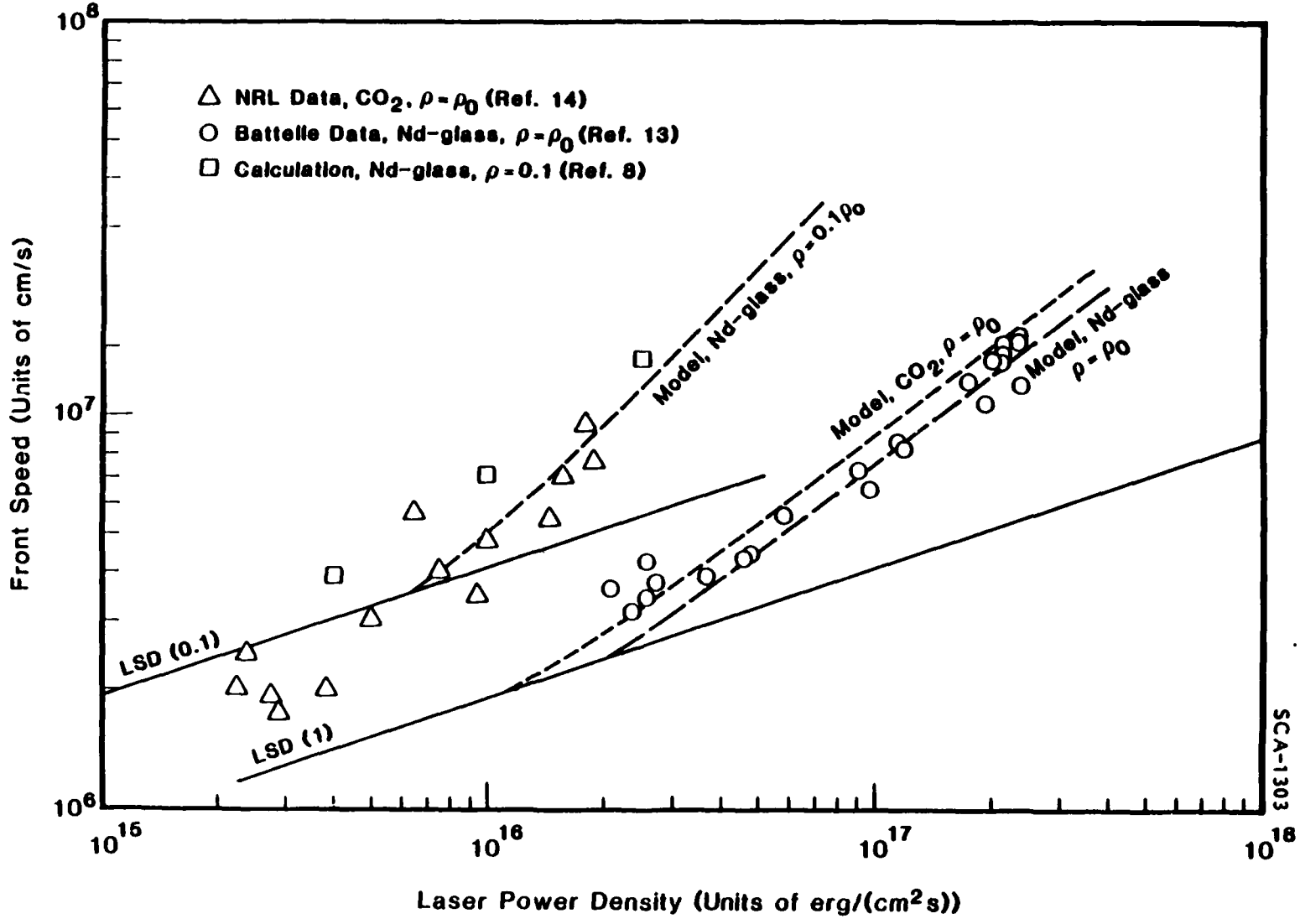

Figure 3. Front speed versus laser power density - comparison of data and calculations.

For comparison with the CO_2 calculations we have also plotted data from NRL experiments[14] in Figure 3. These points (open triangles) represent the maximum frontal speed as a function of peak laser power density deduced from streak camera records. The data, taking into account a large variance about a mean value, are located at much smaller power densities than the model predictions. It is interesting, however, that the slope of the mean curve of speed versus power density is substantially the same as that of the model.

3.2 NUMERICAL CALCULATIONS OF LSR WAVES.

The theoretical curves of Figure 3 are based on an assumed steady-state frontal motion; this theory does not indicate how much time is required to establish the steady-state. When two modes, such as the LSD and the LSR, have similar propagation speeds we expect that the one having the higher speed will ultimately be predominant. Near the intersection of the characteristic curves of the two modes transient behavior is likely to last for a longer time; consequently, in a time-dependent pulse there may not be time to approach a steady-state under these circumstances. Questions regarding transiency and model validity can be resolved by finite difference calculations.

We have identified an existing S-CUBED computer code, called ZOOS, to perform the initial calculations. This code is readily adaptable to the required calculations when provided with appropriate properties of air and with a laser energy absorption subroutine. Several modifications of the radiative transfer portion of the computer code were also made in order to simulate the target interaction problem.

The ZOOS computer code is a flexible, one-dimensional hydrodynamics/radiation formulation applicable to a wide range of high energy applications. The code is basically a Lagrangian, explicit,

transient, finite difference hydrodynamics formulation to which additional physical processes have been added. Shock waves in this formulation are treated by the pseudo-viscosity method. For the application to the interaction of a high-power laser beam with an air plasma formed at a target surface, the plane geometry version of the code was selected. The radiative transfer is the most important of physical processes taking place for the description of the LSR and consequently was given special attention. The formulation assumes that scattering is negligible, and that the radiation intensity is independent of the angle of azimuth about the direction normal to the slab, therefore depending only on the polar angle. A discrete ordinate angular formulation is used. The polar angles are selected as those appropriate for double Gaussian angular quadrature; the order of the quadrature is selected at the option of the user. The subroutine, PTRANS, containing this treatment is carefully formulated to account for exponential attenuation of rays and to recover the diffusion approximation when the medium is thick and the radiation and material are in quasi-equilibrium. The frequency dependence is treated by characterizing the spectrum by a number of fixed-frequency groups to which optical properties are assigned.

Material properties of the medium in question (air, in our calculations) are supplied to the ZOOS code through subroutines. These consist of thermodynamic quantities, including the material energy and its derivatives and the pressure, and optical properties. The latter consist of absorption coefficients of air for each of the frequency groups as a function of temperature and density. In the calculations reported below the thermodynamic, absorption and radiation emission coefficients are all assumed to be given by the local thermodynamic equilibrium values.

The laser beam source is treated separately from the self-radiation of the air plasma. A separate source routine was developed

in which the beam attenuation is calculated as function of the absorption coefficient appropriate to the laser frequency. (The absorption coefficients resulting from laser frequencies ~1 eV and below are described in Section 2.) Oblique incidence of the beam on the surface is treated by accounting for increased path length in the air and by appropriately modifying the beam power; this does not invalidate the assumption of azimuthal independence of the self-radiation intensity.

Calculations were performed with the ZOOS code to determine the optimum choices of parameters associated with the finite difference zoning and number of angles of the angular quadrature. Subsequently, the following calculation was performed for a pulsed Nd-glass laser incident normally on a target in air. Parameters were selected to compare with the analytic model:

1. Laser Pulse Characteristics: (normally incident on target).

   Power -- 10^{10} w/cm^2,

   Wavelength -- 1.06 μm (Nd-glass),

   Duration -- 10 nanoseconds (ns),

   Shape -- Step-function.

2. Target-Air Characteristics:

   Target - ideal reflective and stationary boundary condition,

   Air initial density -- 1.2×10^{-3} gm/cm^3,

   Air temperature -- 10^{-5} gm/cm^2 adjacent to target preheated to 5.0 eV, remainder at ambient.

3. Numerical Discretization:

   Equations -- Lagrangian (mass-following) coordinate,

Zoning -- 2 x 10^{-6} gm/cm^2 (constant) per zone,

Number of Zones -- 70,

Angular Resolution of Radiation -- 6 discrete angles,

Frequency Resolution of Radiation -- 19 groups.

The calculation was carried forward in time to 15 ns, a time 50 percent greater than the pulse duration. Consequently, phenomena relating to starting and stopping transients are displayed by the calculation. In addition, the pulse has a duration which is long enough to display quasi-steady behavior; this portion of the calculation can be compared with the analytic solution of a steady wave interaction.

The results are characterized by the rapid (~2 ns) formation of a self-radiation supported precursor in the initially unheated air traveling toward the laser source. A large peak of 17 eV in temperature is observed near the target surface. This peak, which decreases with time, was formed by the initial laser beam heating of the outer-most zone of the postulated hot layer at the target surface. This absorbing zone protected the zones adjacent to the target from direct laser heating. The peak temperature zone is slowly cooling, and the protected zones are slowly heating by radiation transfer within the air. This process is dependent in detail on the model of initial heating and does not affect the behavior of the LSR wave in any substantial degree.

As the precursor temperature reaches ~2 eV the laser beam energy is absorbed, creating an intense and sharp heating front. This front gradually approaches a steady motion having a temperature plateau of ~10 eV behind it and a speed of ~7 x 10^6 cm/s. The shock wave and following rarefaction wave in the interior of the LSR originate in the initial interaction with the target. They propagate outward with a speed approximately one half of that of the temperature jump. A localized peak in temperature is associated with the shock

front, but strong radiation cooling of the front reduces the amplitude of the peak to ~1 eV. Consequently, the body of the propagating wave is approximately isothermal. The strength of the shock is slowly decreasing due to this radiation damping. The speed of the LSR wave gradually increases over a period of an additional ~2 ns during which the emissive power of the high temperature region approaches unity. Further increase in the wave thickness has little effect on the progress and form of the wave front. After source termination a stronger hydrodynamic disturbance forms in the vicinity of the decaying front. This wave propagates as a shock into the precursor region and as a rarefaction into the region behind the front. The sharp temperature front dissipates rapidly due to diffusion from the frontal region into the precursor region. This combined shock and diffusion wave propagates less rapidly than the laser-supported front. The calculation was terminated before the signals from the front due to the laser beam shut-off were able to reach the target.

In Figure 4 the progress of the laser-supported front is shown. The speed of this front increases to ~7.5×10^6 cm/s, in remarkable agreement with the corresponding case calculated analytically in Reference 12. In Figure 5 the profile of temperature at a time (8.0 ns) before the source is terminated is displayed. It indicates that the temperature behind the front is roughly constant and that the temperature precursor extends ~0.5 mm ahead of the front. There are oscillations of density behind the front (and corresponding pressure oscillations) indicating that hydrodynamic transients characteristic of the initial conditions and the source profile are propagating through the wave. The net flux due to the self-radiation of the air is indicated in Figure 6 for same time. These hydrodynamic disturbances also appear in Figure 7 showing the time dependence of the pressure at the target interface. The peak of the pressure curve results from the delayed arrival at the surface of the shock wave from the initial beam deposition in the preheated air. The final plateau pressure of ~ 2.6 kb represents the steady LSR interaction; transients associated with beam termination have not yet influenced the surface.

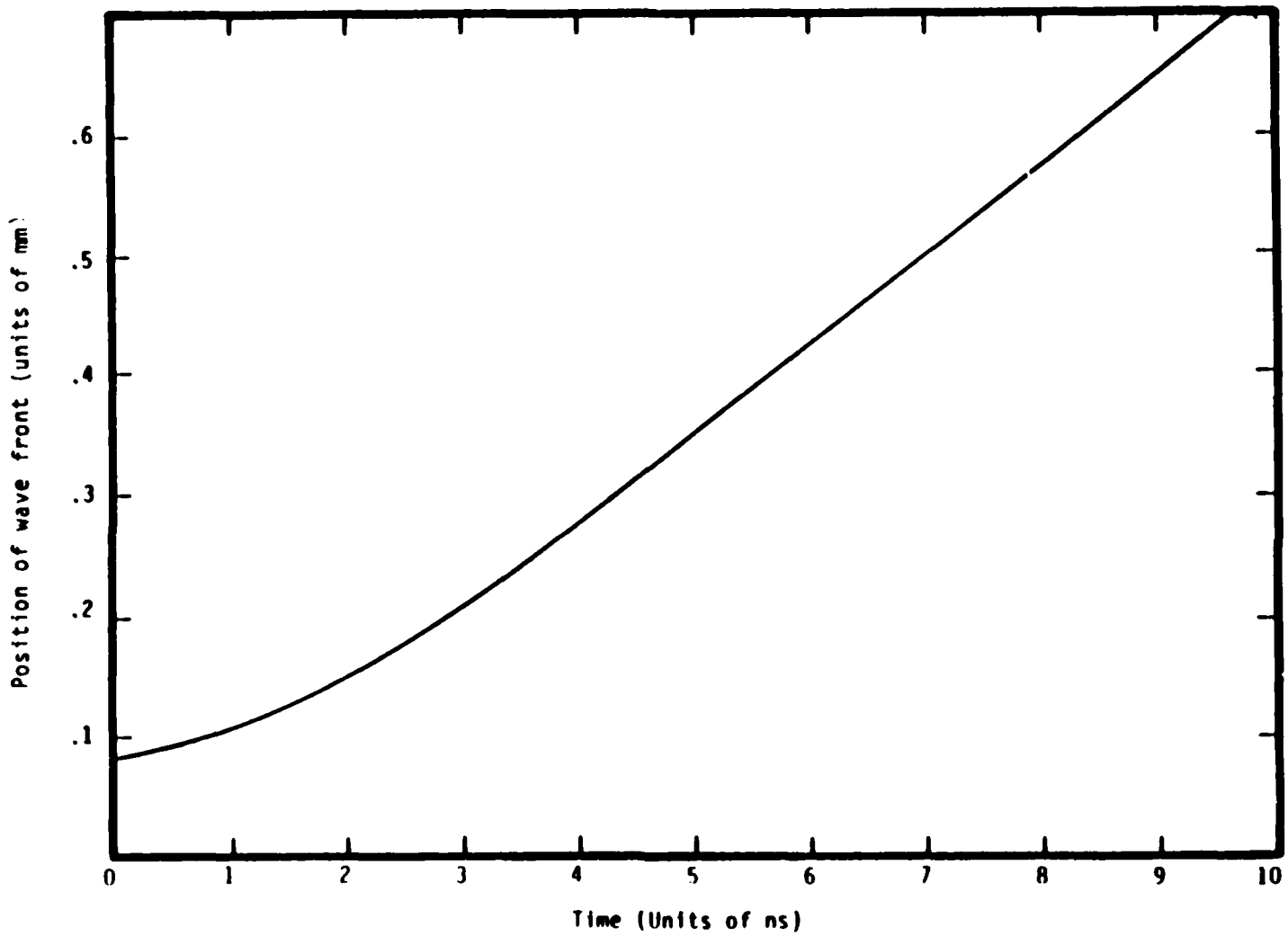

Figure 4. Distance of heating wave front from target versus time.

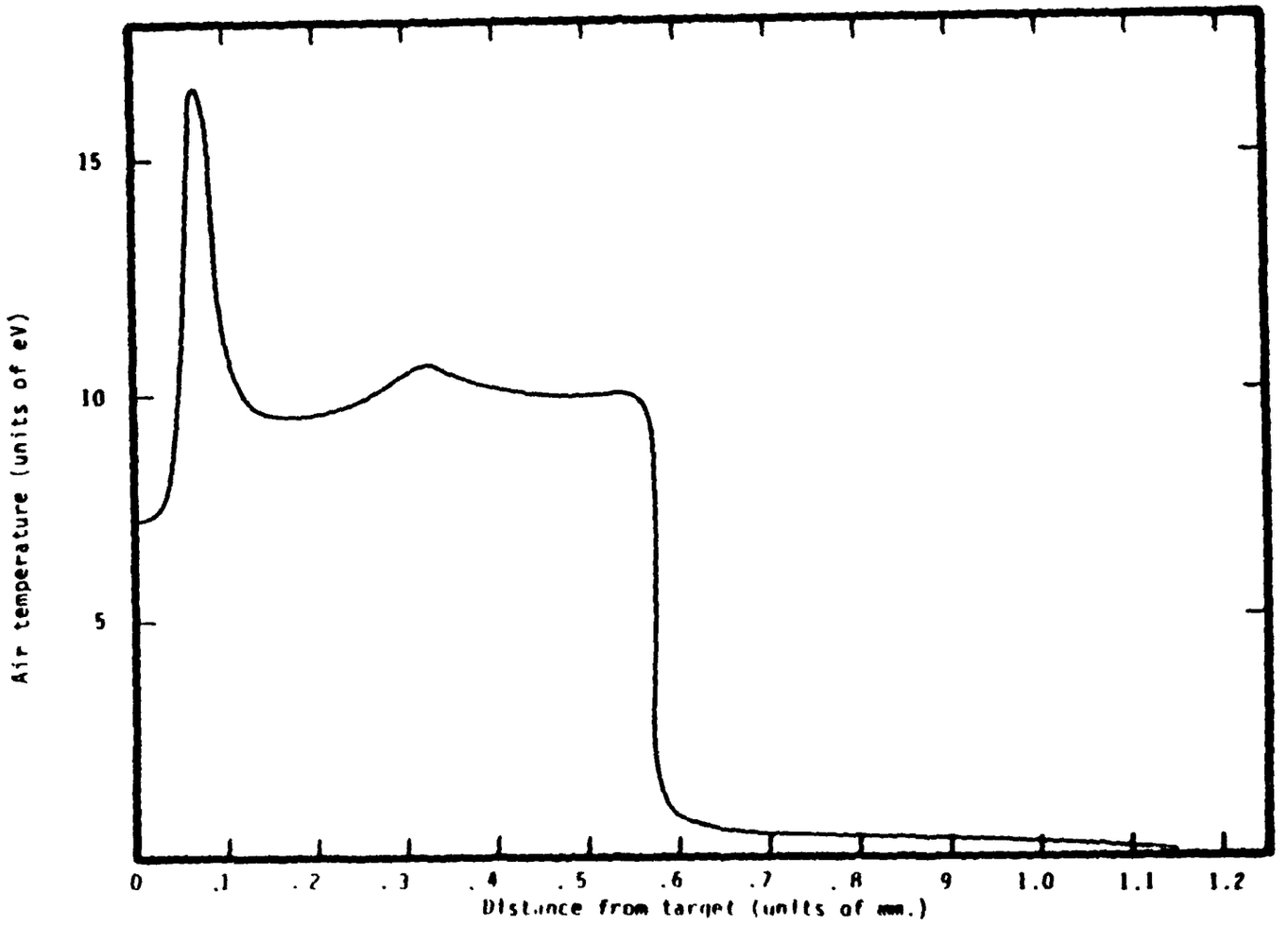

Figure 5. Temperature versus distance from target at time of 8 ns.

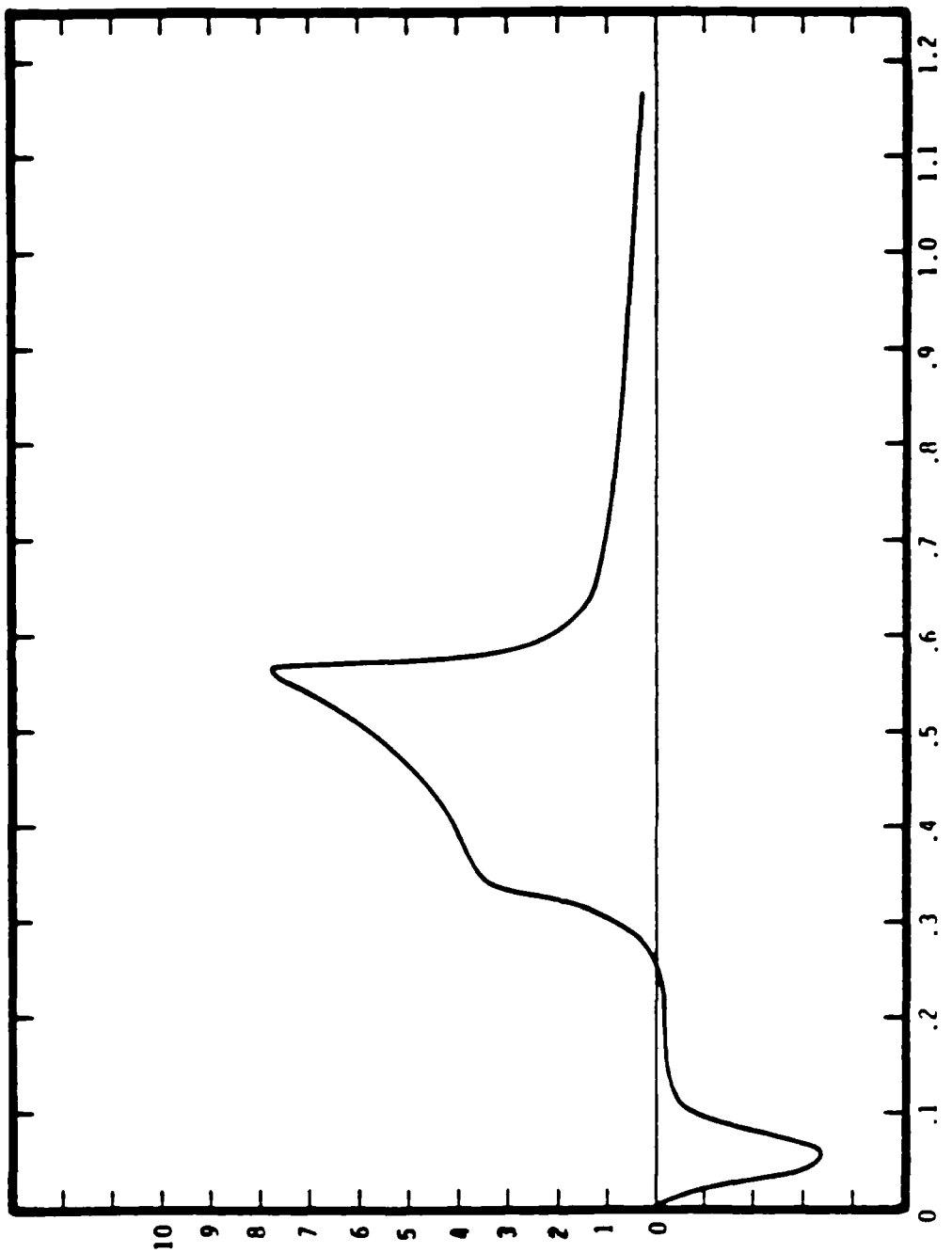

Figure 6. Radiation flux versus distance from target at time of 8 ns.

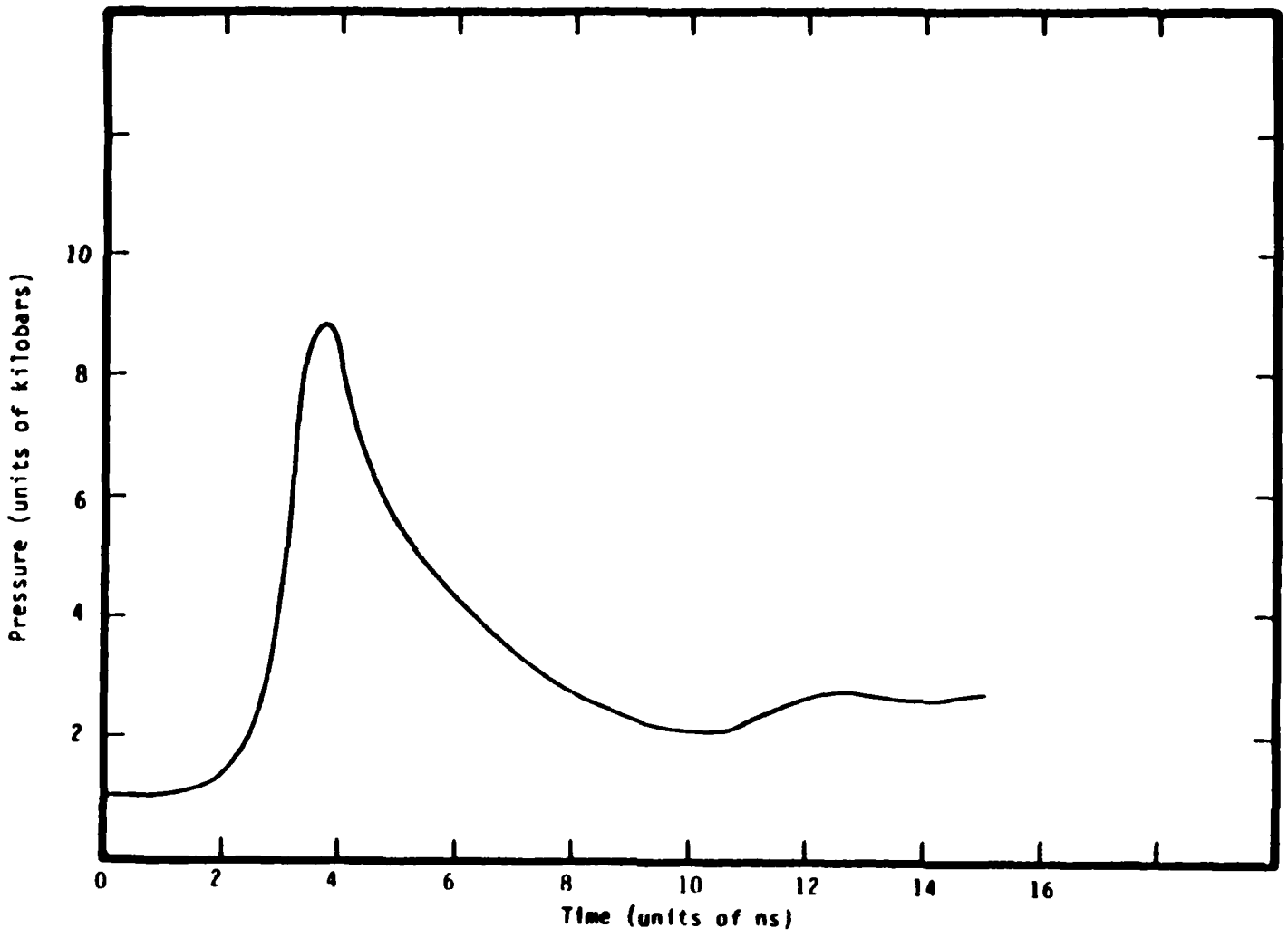

Figure 7. Pressure at target surface versus time.

SECTION 4
DISCUSSION

An investigation of several problems associated with high-power laser interaction with a target has been carried out. Two models of the laser-supported radiation (LSR) mode of wave propagation in air have been developed. The first, an analytic model, describes the dependence of wave properties in a steady-state on laser power and frequency and on air density. The second, a numerical model, is capable of exploring transient effects and target ablation. Comparisons of these model predictions with experimental data have been made.

Applied to sea level density air and Nd-glass laser radiation, the steady-state analytic model predicts that the LSR wave propagates faster than the LSD wave for speeds greater than 2.4×10^6 cm/s. The wave speed of the LSR increases with the 0.71 power of the laser power, while that of the LSD increases with the 0.33 power. As shown in Figure 3, the larger power dependence is qualitatively indicated by high power experimental data, although data just above the transition from the LSD ($2\text{-}3 \times 10^9$ w/cm^2) lie above the curve. The analytic model predicts not only the slope, but also the magnitude of the data. A calculation was also carried out corresponding to the above conditions and having a power of 10^{10} w/cm^2 using the numerical model. Transients associated with the initiation and termination of the laser beam and the initial conditions for the plasma were observed in the calculation. The air propagation requires ~ 2ns to start, during which a shock wave travels into the air and starts to interact with the target. An additional ~ 2ns are required for the LSR to approach a steady-state and for the peak transient target interaction to take place. While the LSR wave and its embedded shock wave are quite steady by 10 ns, the surface pressure is still adjusting to initial conditions. The termination of the laser pulse at 10 ns immediately

initiates a slow-down and diffusion of the LSR front, but by 15 ns its effect has not yet reached the target.

Calculations were also carried out using the analytic model for a Nd-glass laser beam against a target in air of one-tenth normal density. The model predicts that the LSR wave predominates for laser power densities greater than ~ 6×10^8 w/cm^2. These results have been compared with transient calculations of Bergelson, *et al.*[8] which span this transition power range. We find that the frontal speeds of the transient calculations are higher by about 40 percent than the model (see Figure 3, squares versus long dashes). This may represent the trend in the transition range for the two modes of propagation to reinforce each other. We also observe that the steady-state model assumptions are less valid for this case than for normal density. It would be interesting to apply our transient calculation to these conditions.

Analytic model calculations were made for a CO_2 laser beam against a target in normal density air. In this case, the model predicts that the LSR wave is initiated at a power density of ~ 10^9 w/cm^2, indicating that the model is not strongly sensitive to the laser frequency. By contrast, data indicate that the LSR wave starts at a power density smaller by about an order of magnitude While there is a large scatter in the data, the indication is that some process of supporting the radiation wave at a lower temperature is taking place.

The source of the discrepancy may lie in our neglect of another, faster, mode for the CO_2 laser wave propagation The clean-air breakdown threshold in CO_2 (~ 3×10^9 w/cm^2) is located near the model-predicted laser flux at which the radiation wave is initiated While the data points lie below the cold threshold, it is quite possible that the precursor preheating of the air or the effect of

impurities in the air could lower it. While we have not investigated this mode of propagation, it is clear that the radiation wave mode for CO_2 will be superceded by some type of breakdown wave. In the case of Nd-glass radiation the threshold for cold-air breakdown ($\sim 3 \times 10^{11}$ w/cm^2) is substantially higher than the flux range of the data and calculations. Consequently, the comparison of the data with model predictions in this case is meaningful.

The laser-supported radiation wave results in lower temperatures for a given laser flux than for the LSD mode. The model predicts these temperatures; they also have a weaker dependence on flux than for the LSD mode. For the case of Nd-glass and standard air density we obtained

$$\theta(\text{eV}) = 0.30 \left[F_L(\text{w/cm}^2)\right]^{0.15} \qquad (1)$$

These calculations could also be compared with luminosity measurements, such as those carried out in the Battelle experiments.

The numerical laser interaction model developed under this contract is now available for use in a wide survey of LSR problems. The computer code containing the model has a capability to take into account effects which were not included in the example calculation reported above. The most important of these is to model the radiative ablation of the target. The vaporization of the target surface and the subsequent hydrodynamics and radiative transfer within the target vapor can be straightforwardly included. In addition, the laser beam pulse shape and angle of incidence can be assigned desired values. Issues of interest include:

1. Effects of several models of plasma initiation on target surface pressure.
2. Effects of laser power duration and pulse shape on surface pressure.

3. Transition between the LSD and LSR modes and associated transiency of propagation.

4. Target radiative ablation effects during LSR propagation.

5. Transition between the predominance of air interaction and target blow-off on target pressure as the air density is reduced.

6. Effects of different experimental gases on LSR propagation.

Calculations relevant to these issues can be carried out for detailed comparison with existing experimental data. These comparisons would further enhance our understanding of the LSR phenomenon and sharpen our appreciation of the validity of the present model.

The numerical model developed under this contract is inapplicable if the geometry departs appreciably from planar. The most serious nonplanar effect is associated with a small beam radius. Given the high observed speeds of frontal propagation and typical pulse durations, a beam diameter of < 1 cm will result in strong lateral perturbations. The laser-heated air will have time to radiate into the adjacent cold air and to expand, thereby reducing the density and beam absorptivity behind the front. A treatment of these effects in two spatial dimensions is feasible using modifications of existing two-dimensional radiation/hydrodynamic computer codes.

SECTION 5

LIST OF REFERENCES

1. Boni, A., F. Su, P. Thomas and H. Musal (1977), "Theoretical Study of Laser-Target Interactions," Science Applications, Inc. Report No. SAI-77-567LJ.

2. Beverly, R. and C. Walters (1976), "Measurement of CO_2-Laser-Induced Shock Pressure Above and Below LSD-Wave Thresholds," *J. Appl. Phys. 47*, 3485-3495.

3. Raizer, Y. (1965), "Heating of a Gas by a Powerful Light Pulse," *Soviet Phys. JETP 21*, 1009-1017.

4. Pirri, A., R. Root, Pugh, Kemp, G. Simons and G. Weyl (1982), Unpublished Report.

5. Markovich, I., I. Nemchinov, A. Pterukhin, Y. Pleshanov and V. Rybakov (1977), "Optical Detonation Waves in Air Propagating Against a Laser Beam," *Sov. Tech. Phys. Lett 3*, 40-42.

6. Boiko, V., V. Danilychev, B. Duvanov, V. Zuorykin, and I. Kholin (1978), "Observation of Supersonic Radiation Waves in Gases Generated by CO_2 Laser Radiation, *Sov. J. Quantum Electron. 8*, 134-135.

7. Markovich, I., I. Nemchinov, A. Petrukhin, Y. Pleshanov and V. Rybakov (1979), "Photodetonation Waves and Supersonic Radiation Waves in Xenon," *Sov. J. Plasma Phys. 5*, 560-565.

8. Bergelson, V., T. Loseva, I. Nemchinov and T. Orlova (1975), "Propagation of Plane Supersonic Radiation Waves," *Sov. J. Plasma Physics 1*, 498-503.

9. Weyl, G., A. Pirri and R. Root (1980), "Laser Ignition of Plasma Off Aluminum Surfaces," AIAA 13th Fluid and Plasma Dynamics Conference, AIAA-80-1319.

10. Dalgaro, A. and N. Lane (1966), "Free-Free Transitions of Electrons in Gases," *Ap. J. 145*, 623-633.

11. Peach, G. (1967), "Free-Free Absorption Coefficients of Nonhydrogenic Atoms," *Mem. R. Astr. Soc. 71*, 1-11.

12. Freeman, B. E. (1983), "Laser-Supported Radiation Waves in Air - Analytic Correlations," S-CUBED Topical Report No. SSS-R-84-6416.

13. Battelle Memorial Laboratory Experiments - Unpublished Data. (Private communication by Craig Walters)

14. Naval Research Laboratory Experiments - Unpublished Data. (Private communication by Evan Pugh).

APPENDIX

SSS-R-84-6416

LASER-SUPPORTED RADIATION WAVES IN AIR-ANALYTIC CORRELATIONS

B. E. Freeman

November 1983

ABSTRACT

A simplified model of the steady propagation of a laser-supported radiation wave in air has been developed. The model is based on the formation of a self-radiation-heated precursor ahead of the laser-heated main wave. Applied to air at sea-level density and Nd-glass frequency, the laser supported radiation (LSR) mode propagates faster than the laser supported detonation (LSD) wave for speeds greater than 2.4×10^6 cm/s. The calculations are in reasonable agreement with data for this case. Model predictions for low density ambient air and for CO_2 laser frequency are not in agreement with data. Reasons for these discrepancies and limitations on the range of applicability of the model are discussed.

LASER-SUPPORTED RADIATION WAVES IN AIR-ANALYTIC CORRELATIONS

B. E. Freeman

November, 1983

INTRODUCTION

A pulsed high-power laser beam directed against a target in air is observed to generate and support a disturbance whose front travels away from the target toward the source. At the highest powers the wave travels faster than expected for a laser-supported detonation (LSD) wave,[1] and is believed to be the result of laser beam absorption in a radiation precursor.

The evidence for the LSR mode of propagation comes principally from measurements of frontal position of the interaction wave, as a function of time. The data show that a wave propagates substantially faster at high laser power density than an LSD wave. At the Battelle Memorial Laboratory a series of recent experiments has been reported[2] indicating for a Nd-glass laser and normal density air, the dependence of speed on laser power density. Data are available on the frontal speed in normal density air using a CO_2 laser at the Naval Research Laboratory.[3] Earlier data on frontal speed in air corresponding to a range of values of air density and laser frequency have been summarized.[4]

The theoretical basis for the LSR wave is more limited. Estimates were made by Raizer[1] that, under conditions permitting lateral energy loss, the LSR frontal speed is not greatly different from that of the corresponding LSD. Subsequently, Bergelson, et. al.,[5] carried out finite difference calculations for a ND-glass laser in air with 0.1 times normal density and a planar interaction geometry. After initial transients, these calculations showed propagation speeds more strongly dependent on power density than the LSD. They also developed a theoretical explanation of the speed dependence on laser power density.

In this paper a model of the wave propagation, generalizing that of Reference 5, is evaluated in order to relate wave speed to laser power density, laser frequency, and air density. The model is based on a steady state frontal motion associated with a constant power density beam. To eliminate effects of plasma multi-dimensionality the beam is assumed to be uniform over lateral distances much larger than the distance the front propagates. The wave profile is qualitatively as follows:

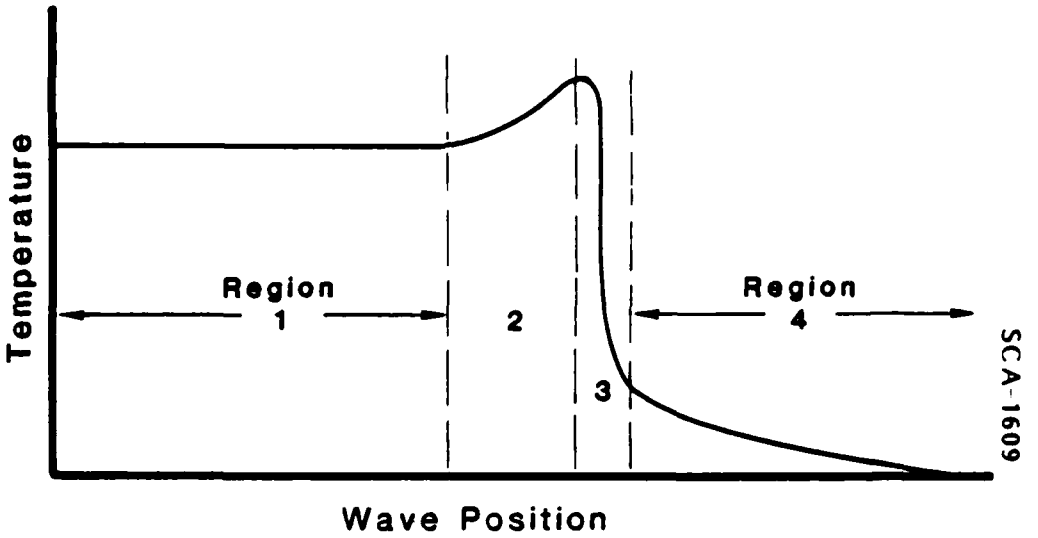

Figure 1.

and is characterized by the four regions of Figure 1:

(1) a uniform region at a distance behind the front,
(2) a region in which the air is cooled by emission of radiation,
(3) a region of intense heating by the laser beam,
(4) a radiation precursor region heated by the photons from region (2).

While the wave-form of Figure 1 is assumed to be steady in the front-following coordinates, a neglected sonic disturbance lagging behind the wave is generated by the interaction of heated air with the target.[6] This interaction affects the pressure experienced by the target.

The model is simplified for calculation by assuming

(1) the laser beam absorption zone is narrow enough to be treated as a discontinuity in the radiation emission calculation;

(2) there is no spontaneous emission in the precursor region;

(3) the speed is determined by equating the air heating rates due to self radiation and laser beam absorption at the interface between regions (3) and (4).

Steady Wave Conservation Conditions

The wave must satisfy the conditions of conservation of mass, momentum and energy in a steady state frame of reference moving with the front. These equations are

$$\rho u = \rho_o u_o \tag{1}$$

$$P + \rho u^2 = \rho_o u_o^2 , \tag{2}$$

$$F + \rho u \left(H + \frac{1}{2} u^2\right) = \frac{1}{2} \rho_o u_o^3 + F_o , \tag{3}$$

where ρ = density

u = velocity in frame moving with the front,

P = pressure

$H = E + P/\rho$ = enthalpy

E = specific internal energy

F = radiation flux (laser plus thermal).

The subscript "o" denotes upstream conditions unperturbed by the wave where the pressure and enthalpy are taken to be negligible. In the

right-facing wave convention of Figure 1, $u_0 = -D$ and $F_c = -F_L + F_x$ where

D = speed of frontal motion

F_L = incident laser flux

F_∞ = thermal radiation flux component normal to target escaping from the wave.

Equations 1-3 can be evaluated in region 1 where $F = C$ and be rearranged to give

$$G = \frac{E}{D^2}\left[1 - \frac{(\gamma - 1)\,\epsilon}{2(1 - \epsilon)}\right], \tag{4}$$

$$\frac{P}{\rho} = D^2\,\epsilon(1 - \epsilon)\,, \tag{5}$$

where $\epsilon = 1 - \frac{\rho_0}{\rho}$, $G = \frac{F_L - F_\infty}{\rho_0 D^3}$ and we used $\frac{P}{\rho} = (\gamma - 1)E$.

Solving (4) and (5),

$$G = \frac{\epsilon}{\gamma - 1}\left[1 - \frac{(\gamma + 1)}{2}\,\epsilon\right]\,, \tag{6}$$

which is shown in Figure 2.

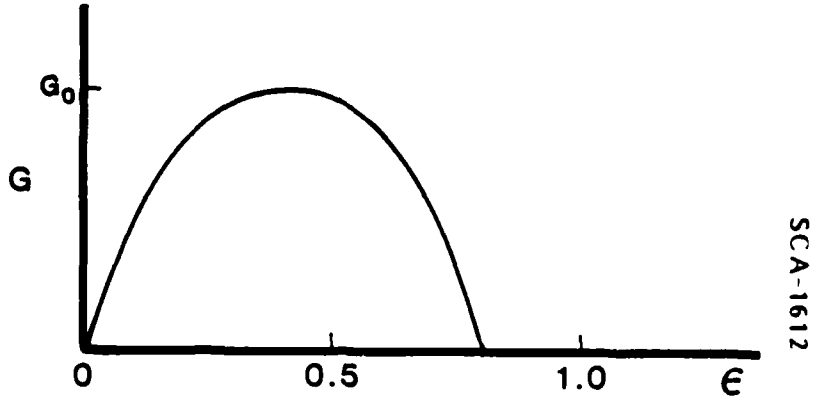

Figure 2.

G has a maximum value, $G_0 = \frac{1}{2(\gamma^2 - 1)}$, at $\epsilon = \frac{1}{\gamma + 1}$, corresponding to the LSD solution. The maximum value of ϵ is $\frac{2}{\gamma + 1}$ which is the strong shock solution. The curve in the range $0 \leq \epsilon \leq \frac{1}{\gamma + 1}$ is obtained for waves which have greater than sonic speed with respect to the gas behind the front. Consequently, these solutions correspond to radiation driven waves having frontal speeds greater than that of the LSD.

Solving for this branch of the quadratic,

$$\epsilon = \frac{1}{\gamma + 1} \left(1 - \sqrt{1 - \frac{G}{G_0}}\right), \tag{7}$$

$$\rho = \frac{(\gamma + 1)\,\rho_0}{\gamma + \sqrt{1 - \frac{G}{G_0}}}, \tag{8}$$

$$E = \frac{2\,G\,D^2}{\gamma + 1} \left(\frac{\gamma + \sqrt{1 - \frac{G}{G_0}}}{1 + \sqrt{1 - \frac{G}{G_0}}}\right) \tag{9}$$

The temperature of the gas, which is a more useful state variable to discuss radiative processes, can be obtained from an equation of state, $\theta = \theta(E, \rho)$. For air in the range of temperatures and densities of interest ($\theta \sim 10$ eV, $\rho \sim \rho_{00} = 1.29 \times 10\text{-}3$ gm/cm^3) an approximate power law equation of state is

$$E = 4.0 \times 10^{11}\, \theta^{1.45}\, (\rho/\rho_{00})^{-0.13} \text{ erg/gm}, \tag{10}$$

where θ is measured in eV.

Self Radiation and Precursor

In Figure 1 we indicate that the beam absorption zone (region 3) is smaller than the cooling zone (region 2). We also assume that the temperature of the toe of the precursor is considerably smaller than that behind the wave. If these conditions are met we expect:

(1) precursor self-radiation to be negligible compared to self-radiation from the main wave,

(2) a reasonable approximation to the self radiation to be $F = \sigma\theta^4$, where θ is the temperature of region 1. (The flux is increased due to the temperature increase of region 2, but decreased by absorption in region 3.)

It is also a good approximation in this problem to:

(3) neglect the radiation emitted into the air transparent window region which escapes to large distances (see appendix),

(4) neglect compression in the precursor (the compression in the main wave is also small for a strongly supersonic wave).

According to the above model the energy equation (9) applied to the toe of the precursor becomes

$$E_p = G\,D^2 = \frac{\sigma\,\theta^4(1 - f)}{\rho_o\,D}\,, \tag{11}$$

where it was assumed that $G = \dfrac{\sigma\,\theta^4 - F_\infty}{\rho_o\,D^3} \ll G_o$ and $f = \dfrac{F_\infty}{\sigma\,\theta^4}$.

Using the equation of state (10), the precursor toe temperature θ_p is determined.

In the precursor the radiation flux decreases by absorption. The spectral intensity I_ν at a distance x ahead of the toe of the precursor is

$$I_\nu = B_\nu \exp(-\tau_\nu/\mu), \qquad (12)$$

where the black body intensity associated with temperature θ is

$$B_\nu = \frac{2h\nu^3}{c^2} \frac{1}{e^{h\nu/\theta} - 1},$$

the optical depth is $\tau_\nu = \int_0^x \mu_\nu' \, dx$, the absorption coefficient corrected for induced emission is $\mu_\nu' = \mu_\nu(1 - e^{-h\nu/\theta})$, and $\mu = \cos\theta$ where θ is the angle between the ray and the normal of the slab. The normal component of the flux F(x) associated with (12) is

$$F(x) = 2\pi \int_0^\infty d\nu \, B_\nu \int_0^1 \mu \, d\mu \exp(-\tau_\nu/\mu) = 2\pi \int_0^\infty d\nu \, B_\nu \, E_3(\tau_\nu), \qquad (13)$$

where the integroexponential $E_n(x) = \int_1^\infty e^{-xy} y^{-n} \, dy$.

At $x = \tau_\nu = 0$

$$F(x = 0) = \pi \int_0^\infty B_\nu \, d\nu = \sigma \theta^4, \text{ as required.}$$

Associated with the flux in the precursor is a rate of heating of the air, which will be required in the determination of the frontal speed. In the absence of precursor compression and assuming no laser heating of the precursor

$$\left.\frac{dE}{dt}\right|_s = -\frac{dF}{dx} = 2\pi \int_0^\infty d\nu \, \mu_\nu' \, B_\nu \, E_2(\tau_\nu). \qquad (14)$$

Evaluated at $x = 0$, the heating rate becomes

$$\left.\frac{dE}{dt}\right|_s = 2\sigma\, \theta^4\, \bar{\mu}\,, \tag{15}$$

where $$\bar{\mu} = \int_0^\infty d\nu\, \mu'_\nu\, (\theta_p,\, \rho_0)\, B_\nu(\theta) \Big/ \int_0^\infty d\nu\, B_\nu\, (\theta),$$

is a mean absorption coefficient similar to the Planck mean, but having greater generality. It depends on the source temperature θ, in addition to the material temperature θ_p and ambient density ρ_0.

Some of the thermal radiation emitted by the main wave will not be absorbed by the precursor and will be effectively lost from the wave. This energy is a small fraction of the total energy, which can be neglected in the dynamics ($f = 0$). The energy loss from the wave is discussed in an appendix.

Laser Beam Heating Rate

According to our model, the precursor is transparent to the beam until the toe temperature is attained. The laser heating rate at the toe, by definition, is equal to that from self radiation:

$$\left.\frac{dE}{dt}\right|_L = -\frac{dF}{dx} = \mu'_L\, F_0\,, \tag{16}$$

where F_0 is the unattenuated laser flux and μ'_L is the absorption coefficient for the laser radiation taking into account the stimulated emission correction. The latter depends on the laser frequency ν_0, the precursor toe temperature θ_p and the ambient density ρ_0.

Optical Properties of Air

In equations (15) and (16) above, absorption coefficients of air for temperatures of a few electron volts and ambient densities are required.

For the laser beam our initial application is to a Nd-glass laser having photon energy $h\nu = 1.16$ eV where the absorption coefficient results from free-free and high-lying bound-free transitions. We have evaluated the absorption coefficient for cases of interest in the absorption of the laser beam. The problem consists of two parts: the evaluation of (equilibrium) concentrations of species, and the calculation of the corresponding absorption coefficients. We have employed results of calculations of the composition of low temperature equilibrium air kindly provided to us by F. Gilmore (private communication). These data include molecular, atomic and ionic species and employ a detailed description of excited states in the partition functions. Using these data as input, a computer code was written to evaluate the contributions of:

(1) free-free transitions in ions,
(2) the correction to account for absorption in high-lying bound states,
(3) free-free transitions in the field of the predominant neutral species (which are important below ~1.5 eV).

This calculation employs the formulation by Dalgarno and Lane[7] for neutral free-free absorption and the corrections to the ionic free-free absorption of N^+ and O^+ by Peach.[8] Data for non-hydrogenic corrections to more highly ionized species are not available; we expect the corrections to be smaller for them and, in any event, to make a smaller contribution to the absorption coefficient in the toe transition region. Molecular band absorption, which may contribute to the absorption coefficient at temperatures less than 1 eV, is currently neglected; the desirability of adding this term will be considered at a later time.

The total absorption coefficient μ_L' evaluated at $h\nu = 1.16$ eV is shown as a function of θ in Figure 3 for standard air density and in Figure 4 for 0.1 times standard density. This quantity is a strongly increasing function of temperature, a property which decreases the sensitivity of the final result to its accuracy. It will be seen below that the most important temperature range for the supersonic wave at standard air density is 1.5 - 2.0 eV. It is also possible to calculate μ_L for other choices of laser frequency and density.

The self-radiation mean absorption coefficient $\bar{\mu}$ of equation (15), a function of θ, θ_p and ρ, is obtained by integration over the frequency spectrum. As noted above, the main wave temperature θ is expected to be substantially larger than the precursor toe temperature. Under the conditions of interest the low frequency absorption will be sensitive to θ_p but the absorption coefficient at higher frequencies around the peak of the Planck spectrum will be substantially independent of θ_p. Since the absorption coefficient is also large in this range, due to strong photoelectric and line absorption, μ is a weak function of θ_p. Line transitions make an important contribution to the opacity since they lie in the UV region where the source is intense and they are fully weighted in the Planck-like mean absorption coefficient.

In order to estimate the dependence of μ on the source temperature, calculations were made using the cold ($\theta_p = 0$) absorption coefficient. We used the data of Stewart and Pyatt[9] for Nitrogen, which includes line transitions. The merged lines effectively extrapolate the absorption to a lower energy than the corresponding photoelectric edge. The quantity μ_ν/ρ_0 (cm^2/gm), shown in Figure 5, does not depend on density. The resulting $\bar{\mu}/\rho_0$ as a function of source temperature is shown in Figure 6; it displays a broad maximum at $\theta \approx 6$ eV. The corresponding curve for air would be expected to be slightly higher. The low-temperature end of the curve will be lowered for increasing θ_p due to ionization.

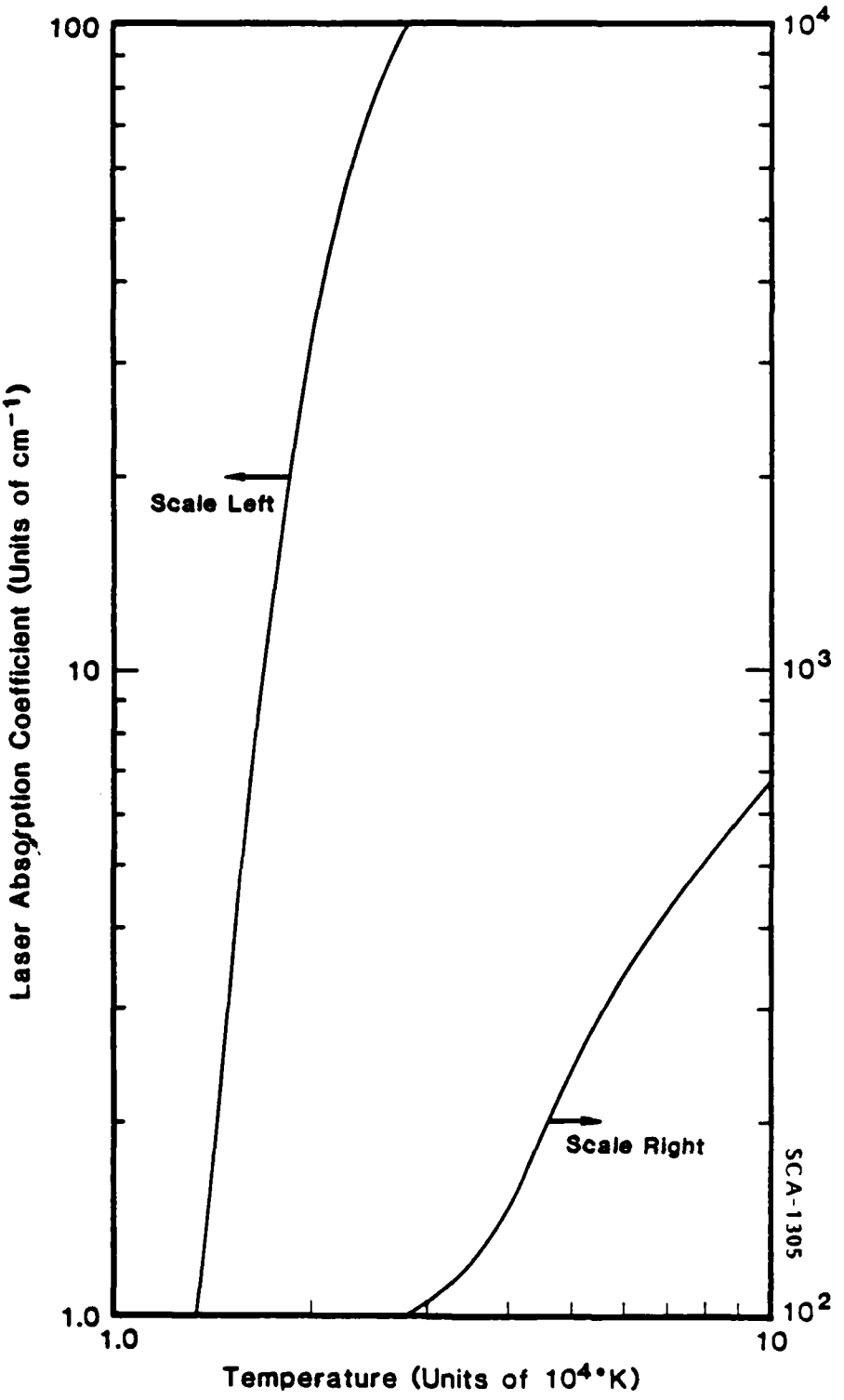

Figure 3. Laser absorption coefficient of air versus temperature for density 1.29×10^{-3} gm/cm^3 and laser frequency = 1.16 eV.

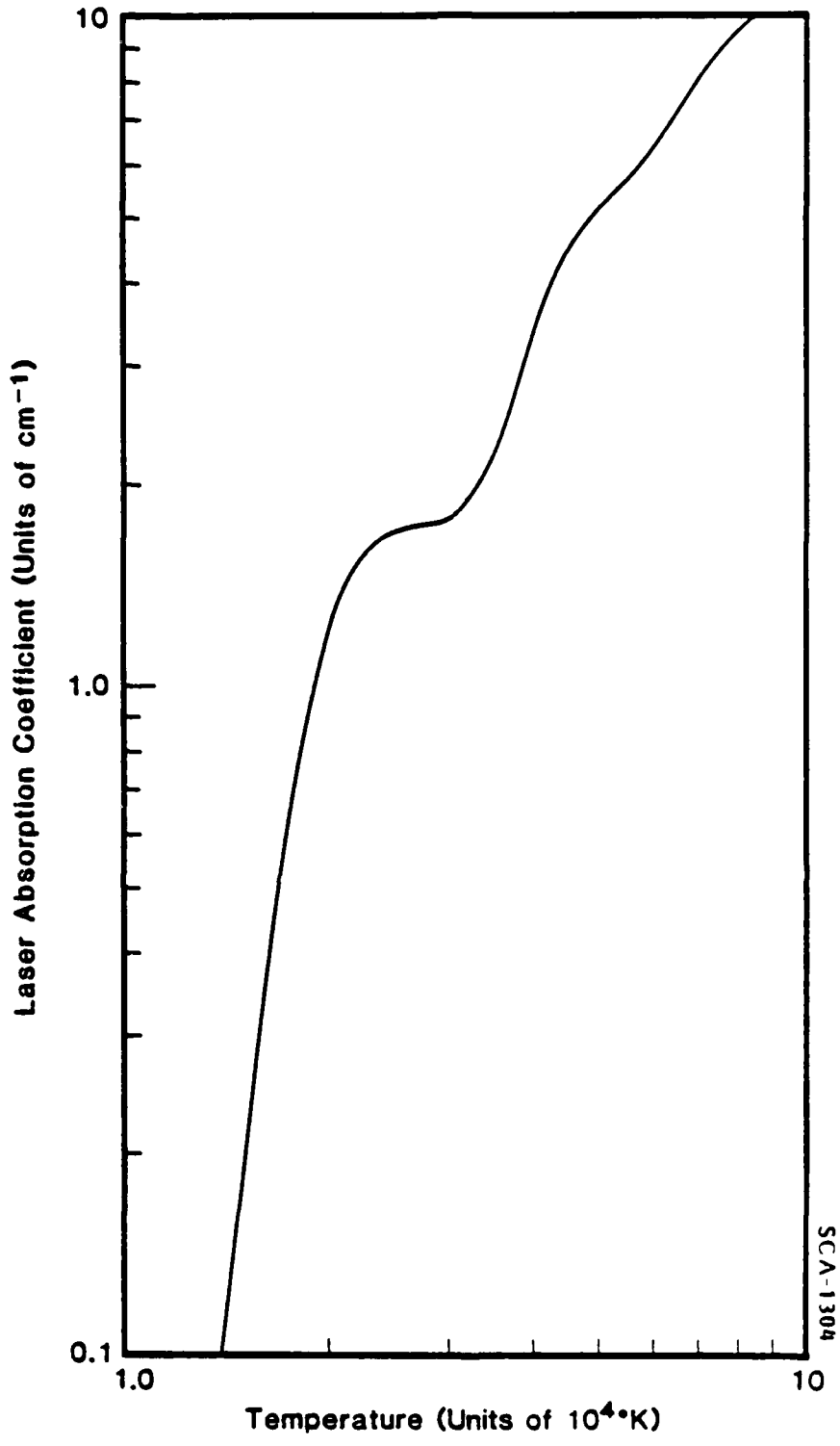

Figure 4. Laser absorption coefficient of air versus temperature for density 1.29×10^{-4} gm/cm^3 and laser frequency = 1.16 eV.

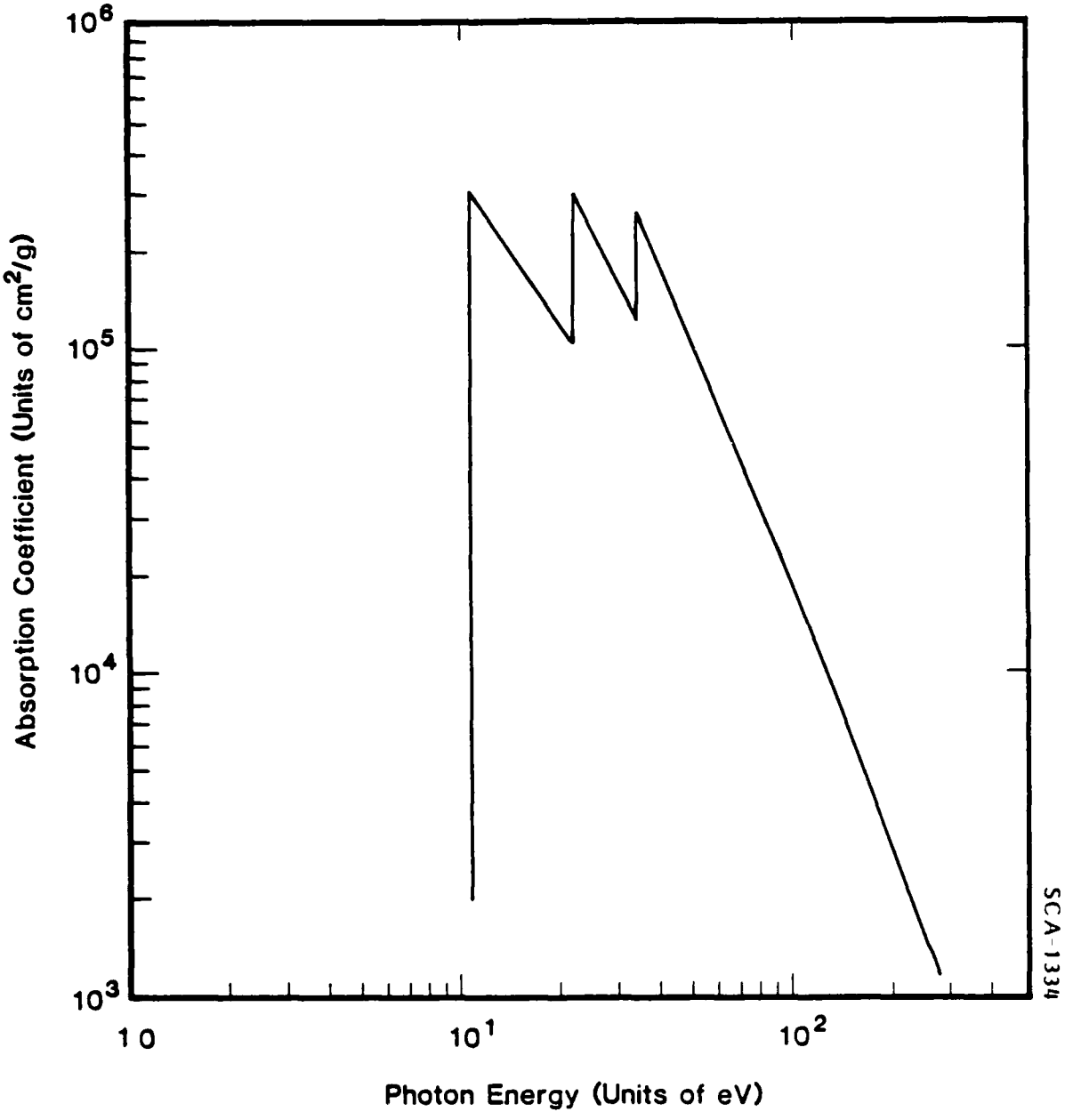

Figure 5. Spectral Absorption Coefficient of Cold Nitrogen Including Smeared Line Absorption.

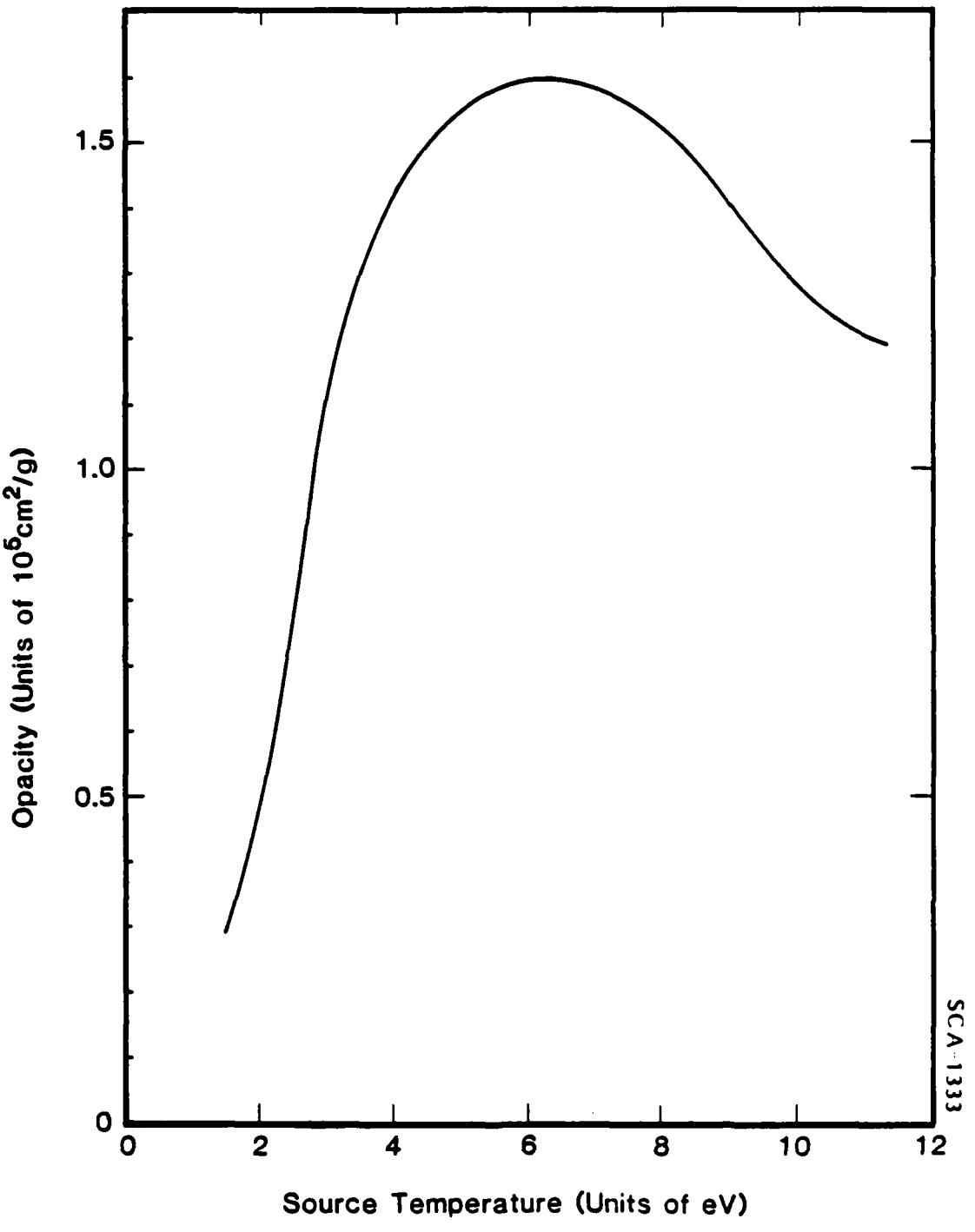

Figure 6. Effective Opacity of Cold Nitrogen for a Black Body Source as a Function of Source Temperature.

Estimates of Wave Speed

Using the above prescriptions, an estimate of the dependence of frontal speed on system parameters (air density and laser power and frequency) can be made, provided an additional relation is added to the conservation equations, (1)-(3). In concert with the model of Figure 1, we require that the toe of the precursor, having temperature θ_p, be defined through the equation:

$$\left.\frac{dE}{dt}\right|_L = \left.\frac{dE}{dt}\right|_s \quad , \tag{17}$$

the terms of which are defined in equations (15) and (16).

In addition to the laser flux, laser frequency and ambient density, they depend on θ_p and θ. The latter temperatures can be evaluated from equations (9) and (11), using equations (10) and (8) for the material energy and wave density. The resulting equation depends on the frontal speed D, in addition to the system parameters; it can be solved for D.

Evaluating these equations for $h\nu = 1.17$ eV (Nd-glass laser frequency) and for $(\rho_0/\rho_\infty) = 0.1, 1.0$ the wave speed dependence on laser flux is shown in Figure 7 (long-dashed curves). Shown for comparison are the corresponding relations for a steady LSD wave (full curves). Also shown (open circles) are data from the experiments of Reference 2, using a Nd-glass laser. The trend of the high-fluence data is reproduced by the model not only in slope but also in magnitude (i.e., there are no adjustable constants within the model; however, the data have been plotted, somewhat arbitrarily, against peak power density). The slope of the theoretical curve for standard density is almost identical with that proposed in Reference 5 on the basis of numerical calculations and a partial theory applied to air of one-tenth normal density. Our calculation for this density displays a steeper slope and is not in good agreement with the calculations of

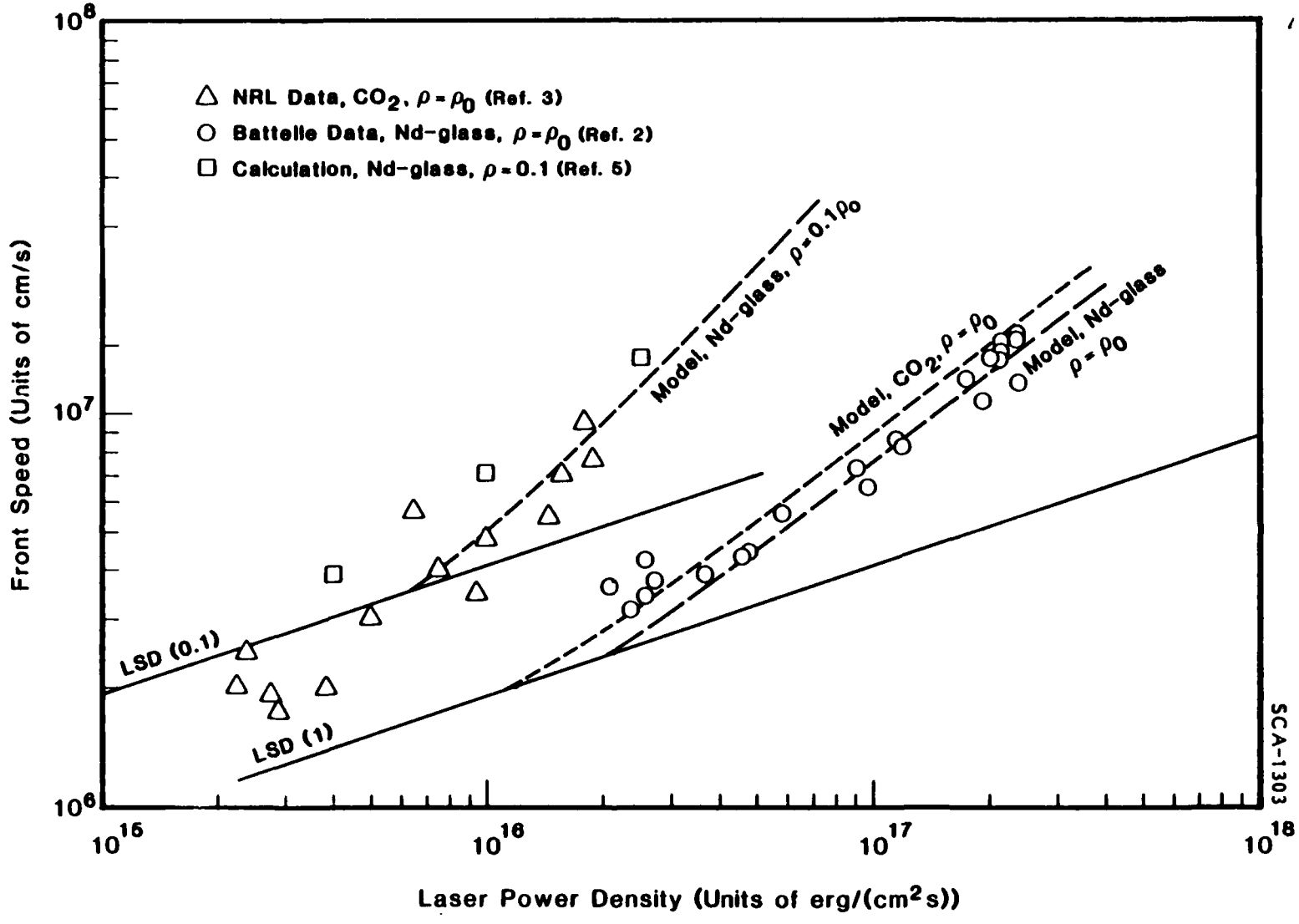

Figure 7. Front Speed vs. Laser Power Density - Comparison of Data and Calculations.

Reference 5 (open squares). Furthermore, in contrast to the normal density case, examination of intermediate results indicates that, especially at the lower flux levels, the assumptions within the model are not well satisfied (the precursor temperature becomes comparable with the main wave temperature). Consequently, the model cannot be confidently applied for Nd-glass at densities of 0.1 normal or less. The apparent agreement between numerical calculations and this type of model in Reference 5 should be regarded with reservations.

The model can be applied at other laser frequencies as well. We carried out a calculation at CO_2 laser frequency (10.6 μm) for standard density air; the result is shown in Figure 7 as the short-dashed curve. The model indicates that the wave speed curve is shifted with aproximately the same slope to somewhat lower power densities. Under these conditions the range of validity of the theory will also extend to somewhat lower densities, because the precursor temperatures are smaller.

For comparison with the CO_2 calculations we have also plotted data from NRL experiments[3] in Figure 7. These points (open triangles) represent the maximum frontal speed as a function of peak laser power density deduced from streak camera records. The data, taking into account a large variance about a mean value, are located at much smaller power densities than the model predictions. It is interesting, however, that the slope of the mean curve of speed vs. power density is substantially the same as that of the model.

The source of the discrepancy may lie in our neglect of another, faster, mode for the CO_2 laser wave propagation. The clean-air breakdown threshold in CO_2 ($\sim 3 \times 10^9$ watt/cm^2) is located near the model-predicted laser flux at which the radiation wave is initiated. While the data points lie below the cold threshold, it is quite possible that the precursor preheating of the air could lower it. While we have not investigated this mode of propagation, it is clear that the radiation wave mode for CO_2 will be superceded by

some type of breakdown wave. In the case of Nd-glass radiation the threshold for cold-air breakdown ($\sim 3 \times 10^{11}$ watt/cm^2) is substantially higher than the flux range of the data and calculations. Consequently, the comparison of the data with model predictions in this case is meaningful.

The laser-supported radiation wave results in lower temperatures for a given laser flux than for the LSD mode. The model predicts these temperatures; they also have a weaker dependence on flux than for the LSD mode. For the case of Nd-glass and standard air density we obtained

$$\theta(\text{eV}) = 0.30 \left[F_L(\text{watt/cm}^2) \right]^{0.15} \qquad (18)$$

These calculations could also be compared with luminosity measurements, such as those carried out in the Battelle experiments.[2]

The theoretical curves of Figure 7 are based on an assumed steady state frontal motion; this theory does not indicate how much time is required to establish the steady state. When two modes of propagation are under consideration we expect that the one having the higher propagation speed will ultimately be predominant. Near the intersection of the characteristic curves of the two modes transient behavior is likely to last for a longer time; consequently, in a time-dependent pulse there may not be time to approach a steady state under these circumstances. Questions regarding transiency and model validity are expected to be resolved by planned finite difference calculations.

The model is also inapplicable if the geometry departs appreciably from planar. The most serious non-planar effect is associated with a small beam radius. Given the high observed speeds of frontal propagation and typical pulse durations, a beam diameter of < 1 cm will result in strong lateral perturbations. The laser-heated air will have time to expand, thereby reducing the density and beam absorptivity behind the front.

The omission of molecular absorption appears to be satisfactory for the cases presently considered; higher ambient air density or lower laser frequency might require their inclusion.

SUMMARY

A model of the laser-supported radiation mode of frontal propagation in air has been developed. The model, based on several assumptions about the shape of the wave, has been evaluated and compared with recently obtained data. In the case of Nd-glass frequency and standard density air the assumptions are justified and the predictions of the model explain the magnitude and trend of the data. In the case of Nd-glass and one-tenth standard air density the assumption of no precursor emission is not satisfied, and the predictions deviate from the results of more detailed calculations. In the case of a CO_2 frequency laser the predictions deviated markedly from measurements.

We speculate that another propagation mode, associated with air breakdown, is responsible for the CO_2 discrepancy; breakdown should not affect the validity of the Nd-glass application of the model. For low density air the model requires modification. Questions regarding the suitability of a steady-state model and of the accuracy of the data have not been resolved. A finite difference formulation of the propagation of the radiation mode wave (under development) will resolve several of the above questions, but do not address th question of effects of deviations from local thermodynamic equilibrium.

RADIATIVE ENERGY LOSS

A wave traveling in air having a high temperature, such as the laser-supported radiation (or detonation) wave, will radiate some of its energy into a relatively transparent spectral window. Energy in this band will be lost from the wave and will not contribute to the interaction impulse. Similar considerations apply in the case of the nuclear blast wave and in the shock wave associated with hypervelocity objects in air, as well as in HE-driven shock tubes.

What constitutes energy lost from the wave depends on the spatial and temporal scale of the problem. The energy deposited in a precursor having a one meter characteristic length will be recaptured by a nuclear blast wave (length scale >> 1 meter), but is effectively lost from the high-energy laser-target interaction, where the length scale is of order 1 cm.

As an example of the radiative structure of a strong wave in air it is instructive to examine a detailed calculation of air shock waves.[10] These show that, for waves into air having standard atmospheric density, and frontal velocities $< 8 \times 10^6$ cm/s, the radiative precursor has components with several characteristic lengths: a component with length scale $\lesssim 0.1$ mm due to photoelectric and line absorption of photons with $h\nu \gtrsim 10$ eV; a component with length scale ~ 1 mm, due to absorption of the O_2 Schumann-Runge (SR) continuum ($7\text{eV} \lesssim h\nu \lesssim 9.7$ eV); and a component with a larger characteristic length for photons with $h\nu < 7$ eV, which exceeds a 1 meter mean free path for $h\nu \lesssim 6$ eV. The low frequency (or window) part of the absorption spectrum is sensitive to the air temperature; heating will reduce absorption in the SR continuum, but the window region will become more opaque. At T = 15,000 K, for example, the mean free path is ≥ 1 cm for $2\text{ eV} \leq h\nu \leq 10$ eV.

The air shock wave calculation[10] shows that at low shock temperatures, $\theta_s \leq 10$ eV, the emitted radiation intensity is approximately that of a black body at the shock temperature; at higher shock temperatures the intensity is reduced by emission from the precursor itself. This result is not strictly applicable to the case of a laser-supported radiation wave because the wave speed for a given temperature is not the same. As indicated by Equation (11), the precursor temperature will tend to be lower, due to a higher wave speed.

Based on the above considerations, an estimate of energy loss in normal density air is obtained from the radiation into the 0 $h\nu$ 7 eV spectral band. Our calculations for this case indicate that the wave temperature increases slowly from ~ 7.5 eV at threshhold (intersection with the LSD wave), to ~ 11 eV at $D = 1.5 \times 10^7$ cm//s. The corresponding precursor temperature decreases from ~ 2.0 eV at threshhold to ~ 1.5 eV. Consequently, the assumptions discussed above should be applicable. Carrying out the indicated calculation, we find that the fraction of incident laser energy lost by reradiation decreases from 0.45% at threshhold to 0.06% at $D = 1.5 \times 10^7$ cm/s. The decreasing fraction with increasing laser power is due to both a decrease in $\sigma\theta^4/F_L$ and a decrease in the fraction of black body flux escaping in the window. An estimate of this kind of energy loss for the case of 0.1 times the standard air density is not accurate because precursor temperatures exceed 5 eV for the cases considered.

Based on the above estimate, the energy lost from the wave by reradiation for standard air density is negligible in the energy balance. Similarly, the reduction in wave pressure and in pressure on the target are also negligible. It should be kept in mind that radiative losses due to small beam diameter have not been considered in this discussion.

REFERENCES

1. Raizer, Yu., 1965: "Heating of a Gas by a Powerful Light Pulse", Sov. Phys. JETP 21, 1009–1017.

2. Battelle Memorial Laboratory experiments - unpublished data. (Private communication by Craig Walters).

3. Naval Research Laboratory Experiments - unpublished data. (Private communication by Evan Pugh).

4. Markovich, I., I. Nemchinov, A. Petrukhin, Y. Pleshanov and V. Rybakov, 1977: "Optical Detonation Waves in Air Propagating Against a Laser Beam", Sov. Tech. Phys. Lett. 3, 40–42.

5. Bergelson, V., T. Loseva, I. Nemchinov, and T. Orlova, 1975; "Propagation of Plane Supersonic Radiation Waves", Sov. J. Plasma Physics 1, 498–503.

6. Triplett, J. and M. Rice, 1983: "Laser Absorption Waves", S-CUBED Memorandum dated 20 September.

7. Dalgaro, A. and N. Lane, 1966: "Free-free Transitions of Electrons in Gases", Ap.J. 145, 623–633.

8. Peach, G., 1967: "Free-free Absorption Coefficients of Non-hydrogenic Atoms", Mem. R. Astr. Soc. 71, 1–11.

9. Stewart, J. and K. Pyatt, 1966: "Theoretical Study of Optical Opacities", Air Force Special Weapons Center Report No. AFSWL-TR-61-71.

10. Zinn, J. and R. Anderson, 1973: "Structure and Luminosity of Strong Shock Waves in Air", Phys. Fluids 16, 1639–1644.

DISTRIBUTION LIST

DEPARTMENT OF DEFENSE

DEF RSCH & ENGRG
ATTN: ENGR TECH J PERSCH

DEFENSE ADVANCED RSCH PROJ AGENCY
ATTN: F PATTEN

DEFENSE INTELLIGENCE AGENCY
ATTN: RTS-2B

DEFENSE NUCLEAR AGENCY
ATTN: SPAS
4 CYS ATTN: TITL

DEFENSE TECHNICAL INFORMATION CENTER
12 CYS ATTN: DD

STRATEGIC DEFENSE INITIATIVE ORGANIZATION
ATTN: R YESENSKY
ATTN: T/SL P TERRY
ATTN: T/SL S GEARY

DEPARTMENT OF THE ARMY

U S ARMY MATERIAL TECHNOLOGY LABORATORY
ATTN: R FITZPATRICK

U S ARMY MISSILE COMMAND
ATTN: W FRIDAY

U S ARMY STRATEGIC DEFENSE COMMAND
ATTN: SDC/S BROCKWAY

DEPARTMENT OF THE NAVY

NAVAL INTELLIGENCE SUPPORT CTR
ATTN: NISC-11 A COBLEIGH

NAVAL POSTGRADUATE SCHOOL
ATTN: PROF K E WOEHLER

NAVAL RESEARCH LABORATORY
ATTN: CODE 4600 D NAGEL
ATTN: CODE 4633 R WENZEL

NAVAL SEA SYSTEMS COMMAND
2 CYS ATTN: PMS
ATTN: R RUDKIN

NAVAL SURFACE WEAPONS CENTER
ATTN: CODE R-31 J THOMPSON

OFFICE OF NAVAL TECHNOLOGY
ATTN: CODE 217

STRATEGIC SYSTEMS PROGRAM OFFICE (PM-1)
ATTN: NSP-L63 (TECH LIB)

DEPARTMENT OF THE AIR FORCE

AIR FORCE CTR FOR STUDIES & ANALYSIS
ATTN: AFCSA/SAMI (R GRIFFIN)

AIR FORCE SYSTEMS COMMAND
ATTN: DLWM

AIR FORCE WEAPONS LABORATORY, NTAAB
ATTN: NTCO C AEBY
ATTN: TA B FREDERICKSON
ATTN: TA E HERRERA
ATTN: TA J WALTON
ATTN: TALE T EDWARDS

AIR FORCE WRIGHT AERONAUTICAL LAB
ATTN: AFWAL/MLP W WOODY
ATTN: B LAINE
ATTN: J RHODEHAMEL
ATTN: MLPJ/DR S R LYON
ATTN: W HARRIS

FOREIGN TECHNOLOGY DIVISION, AFSC
ATTN: A CORDOVA

SPACE DIVISION/YN
ATTN: YNS D RUBERA

DEPARTMENT OF ENERGY

EG&G IDAHO INC
ATTN: J EPSTEIN

UNIVERSITY OF CALIFORNIA
LAWRENCE LIVERMORE NATIONAL LAB
ATTN: F SERDUKE
ATTN: H KRUGER
ATTN: M GERRISSIMENKO

LOS ALAMOS NATIONAL LABORATORY
ATTN: A GREENE
ATTN: T KING
ATTN: R S DINGUS
ATTN: J PORTER

SANDIA NATIONAL LABORATORIES
ATTN: M BIRNBAUM

SANDIA NATIONAL LABORATORIES
ATTN: DR J POWELL
ATTN: K MATZEN

DEPARTMENT OF DEFENSE CONTRACTORS

ACUREX CORP
ATTN: B LAUB

AEROSPACE CORP
ATTN: H BLAES
ATTN: R COOPER
ATTN: T PARK

APTEK, INC
ATTN: DR E FITZGERALD

BATTELLE MEMORIAL INSTITUTE
ATTN: C WALTERS

GENERAL RESEARCH CORP
ATTN: R PARISSE

GENERAL RESEARCH CORP
ATTN: J SOMMERS

HAROLD ROSENBAUM ASSOCIATES, INC
ATTN: G WEBER

JAYCOR
ATTN: DR M TREADAWAY

KAMAN SCIENCES CORP
ATTN: J CARPENTER
ATTN: R ALMASSY

KAMAN TEMPO
ATTN: DASIAC

KAMAN TEMPO
2 CYS ATTN: DASIAC

KTECH CORP
ATTN: D KELLER

MCDONNELL DOUGLAS CORP
ATTN: D JOHNSON
ATTN: J S KIRBY
ATTN: L COHEN

PACIFIC-SIERRA RESEARCH CORP
ATTN: H BRODE, CHAIRMAN SAGE

PHYSICAL SCIENCES, INC
ATTN: A PIRRI

PHYSICS INTERNATIONAL CO
ATTN: M KRISHNAN

R & D ASSOCIATES
ATTN: B GOULD
ATTN: D GAKENHEIMER
ATTN: F A FIELD
ATTN: P A MILES

RAND CORP
ATTN: E HARRIS

S-CUBED
2 CYS ATTN: B FREEMAN
2 CYS ATTN: P. PATNAIK
ATTN: G GURTMAN

SCIENCE APPLICATIONS INTL CORP
ATTN: H JANEE

SPARTA, INC
ATTN: J E LOWDER
ATTN: R G ROOT

SRI INTERNATIONAL
ATTN: B HOLMES
ATTN: D CURRAN
ATTN: G ABRAHAMSON

TRW ELECTRONICS & DEFENSE SECTOR
ATTN: F FENDELL

W J SCHAFER ASSOCIATES, INC
ATTN: J REILLY

END

7-87

DTIC